

2

AD-A239 384



NAVSWC TR 91-409

FORECASTING GEOPOTENTIAL TRENDS IN SOUTHERN GREENLAND

BY JAMES P. CUNNINGHAM PATRICK J. FELL
STRATEGIC SYSTEMS DEPARTMENT

JULY 1991

Approved for public release; distribution is unlimited.



NAVAL SURFACE WARFARE CENTER

Dahlgren, Virginia 22448-5000 • Silver Spring, Maryland 20903-5000

91-07401



NAVSWC TR 91-409

**FORECASTING GEOPOTENTIAL TRENDS
IN SOUTHERN GREENLAND**

**BY JAMES P. CUNNINGHAM PATRICK J. FELL
STRATEGIC SYSTEMS DEPARTMENT**

JULY 1991

Approved for public release; distribution is unlimited.

**NAVAL SURFACE WARFARE CENTER
Dahlgren, Virginia 22448-5000 • Silver Spring, Maryland 20903-5000**

FOREWORD

This report describes the results of a study to model the mass distribution of southern Greenland from an assortment of geophysical data for the purpose of predicting trends in the geopotential. The work was performed in the Space and Surface Systems Division of the Strategic Systems Department.

This report has been reviewed by J. L. Sloop, Head, Space and Surface Systems Division.

Approved by:

R. L. Schmidt

R. L. SCHMIDT, Head
Strategic Systems Department



Accession For	
NTIS GEM&I	<input checked="" type="checkbox"/>
DTIC TAB	<input type="checkbox"/>
Unannounced	<input type="checkbox"/>
Justification	
By	
Distribution/	
Availability Codes	
Avail and/or	
Dist	Special
A-1	

ACKNOWLEDGEMENTS

The authors would like to thank Walter J. Groeger and C. Harris Seay for their support during the analysis of the data and Gary L. Sitzman, who contributed guidance and encouragement throughout the entire effort. Researchers at NASA Goddard Space Flight Center, H. Jay Zwally and Robert A. Bindschadler, and Anita C. Brenner of ST Systems Corporation added helpful commentaries and remarks to the SEASAT and GEOSAT data they provided. Claire Hanson of the World Data Center-A for Glaciology provided the data catalogues containing the Danish radio echo soundings.

CONTENTS

	<u>Page</u>
INTRODUCTION	1
GEOPHYSICAL DATA SOURCES	2
SATELLITE RADAR ALTIMETRY	2
RADIO ECHO SOUNDINGS	4
GEOLOGICAL MAP	5
GRAVITY ANOMALIES	5
METHODS	6
SURFACE ELEVATION GRIDS	6
GEOPOTENTIAL MODELING	7
RESULTS	9
COMPOSITE TOPOGRAPHIC DATA BASE	9
GRAVITY DISTURBANCE AND VERTICAL DEFLECTION	
TRENDS IN SOUTHERN GREENLAND	9
COMPARISON OF GEOPOTENTIAL FORECASTS WITH	
FREE-AIR ANOMALY DATA	10
CONCLUSIONS	13
REFERENCES	13
DISTRIBUTION	(1)

ILLUSTRATIONS

<u>Figure</u>	<u>Page</u>
1 GRID OF SURFACE ELEVATIONS DERIVED FROM SEASAT RADAR ALTIMETRY	16
2 GRID OF SURFACE ELEVATIONS DERIVED FROM GEOSAT RADAR ALTIMETRY	16
3 TRACK DISTRIBUTION OF DANISH RADIO ECHO SOUNDINGS ..	17
4 EXAMPLE OF DANISH RADIO ECHO SOUNDINGS PROFILE	17
5 NRL GRAVITY ANOMALIES	18
6 DMAAC GRAVITY ANOMALIES	18
7 LOCATIONS OF MANUALLY EDITED DATA	19
8 DUAL PRISM MODELS WITH COMMON BASES FOR SURFACE AND BEDROCK MASS DISTRIBUTIONS	19
9 CONTOUR OF SURFACE ELEVATIONS FOR SOUTHERN GREENLAND	20
10 3D PERSPECTIVE OF SURFACE ELEVATIONS OF SOUTHERN GREENLAND	20
11 CONTOUR OF BEDROCK ELEVATIONS FOR SOUTHERN GREENLAND	21
12 3D PERSPECTIVE OF BEDROCK ELEVATIONS OF SOUTHERN GREENLAND	21
13 CONTOUR OF SURFACE ELEVATIONS BASED ON DANISH SOUNDINGS	22
14 COMPARISONS OF ELEVATIONS OF TWO ICE SURFACES: COMPOSITE VS DANISH	22
15 GRAVITY DISTURBANCE AT 3800 M BY TOPOGRAPHIC REDUCTION	23

ILLUSTRATIONS (CONTINUED)

<u>Figure</u>		<u>Page</u>
16	VERTICAL DEFLECTION ξ AT 3800 M BY TOPOGRAPHIC REDUCTION	23
17	VERTICAL DEFLECTION η AT 3800 M BY TOPOGRAPHIC REDUCTION	24
18	3D PERSPECTIVE OF GRAVITY DISTURBANCE AT 3800 M	24
19	NRL GRAVITY ANOMALY PROFILE NEAR 70.4° N	25
20	ACTUAL ANOMALY VS SIMULATED DISTURBANCE ALONG NRL PROFILE	25
21	DMAAC GRAVITY ANOMALY PROFILE NEAR 66.4° N	26
22	ACTUAL ANOMALY VS SIMULATED DISTURBANCE ALONG DMAAC PROFILE	26
23	NRL GRAVITY ANOMALY PROFILE NEAR 70.5° N	27
24	ACTUAL ANOMALY VS SIMULATED DISTURBANCE ALONG NRL PROFILE	27
25	GÅSEFJORD LOCATION OF NRL FREE-AIR ANOMALIES	28
26	GÅSEFJORD DISTRIBUTION OF NRL FREE-AIR ANOMALIES	28
27	GÅSEFJORD 3D PERSPECTIVE OF FREE-AIR AND SIMULATED GRAVITY	29
28	MODEL COMPARISON IN GÅSEFJORD AREA	29
29	HOLSTEINSBORG LOCATION OF NRL FREE-AIR ANOMALIES	30
30	HOLSTEINSBORG DISTRIBUTION OF NRL FREE-AIR ANOMALIES	30
31	HOLSTEINSBORG 3D PERSPECTIVE OF FREE-AIR AND SIMULATED GRAVITY	31

ILLUSTRATIONS (CONTINUED)

<u>Figure</u>		<u>Page</u>
32	JAMESON LAND LOCATION OF NRL FREE-AIR ANOMALIES	31
33	JAMESON LAND DISTRIBUTION OF NRL FREE-AIR ANOMALIES	32
34	JAMESON LAND 3 ^D PERSPECTIVE OF FREE-AIR AND SIMULATED GRAVITY	32

INTRODUCTION

During the summer seasons of 1991 and 1992, the Naval Research Laboratory (NRL) and the Naval Oceanographic Office in collaboration with researchers from the National Oceanic and Atmospheric Administration and the National Survey and Cadastre of Denmark will perform a detailed airborne survey of Greenland to map gravity, magnetics, and the topography of the entire island. During the first summer campaign, southern Greenland, below 70° N, will be surveyed with the NRL P-3 Orion aircraft equipped with LaCoste-Romberg and Bell gravimeters, radar and laser altimeters, Global Positioning System (GPS) receivers, and a proton-precession magnetometer. After processing of the GPS data to remove radial accelerations of the aircraft, it is anticipated that the gravity field will be recovered with an rms accuracy of 2 mgal for half-degree means. Along-track wavelength resolution should be on the order of 25-40 km.¹

Because of the sparse distribution of gravity data within Greenland, the current mean anomaly field, primarily based on prediction,² fails to replicate trends in the observed geopotential field. To better forecast trends, a project was initiated at the Naval Surface Warfare Center (NAVSWC) to collect and exploit higher resolution and more complete geophysical data sources. Such improved predictions could support survey design and assist in the interpretation of data acquired from the airborne survey. The result of this effort is a composite topographic data base that supports the prediction of intermediate wavelengths in the geopotential field. A more complete model of the geopotential would require a detailed description of the island's geology which, unfortunately, is well-known only in the coastal ice-free areas. However, using available data Haller³ has postulated a general description of the island's geology.

The island of Greenland is part of the Precambrian shield of North America. Two Paleozoic fold belts eroded and then uplifted by more recent tectonic activity in the coastal areas envelop the old crystalline block. The Paleozoic plane of erosion in the center of the island may be underlain by two northward-tilting basement blocks separated by a distinct depression near 70° N. The age of the depression may be similar to the age of the coastal tectonic uplift. More recent than the tectonic uplift, isostatic uplift began following partial removal of the Pleistocene ice sheet.⁴ The balance of that ice sheet, which averages 1.5 km thick over most of the island,⁵ reaches its maximum thickness of more than 3100 m near 72° N. Sizable physiographic features such as these make significant wavelength contributions to the geopotential model because their gross surfaces are well defined by the topographic data base.

In the sections that follow, the data sources collected during the project are described. The later sections address the development of the composite topographic data base, geopotential forecasting using the inferred mass distribution, and model evaluations.

GEOPHYSICAL DATA SOURCES

Various data types collected for the Greenland area were used to generate surface elevations of the ice sheet and underlying bedrock. Other data sources were used to evaluate predictions of geopotential trends in southern Greenland. Data sources for both of these purposes are discussed.

SATELLITE RADAR ALTIMETRY

The SEASAT and GEOSAT satellite radar altimeters were designed to measure the ocean surfaces to recover the gravity field at sea and mesoscale oceanographic features. New techniques developed by NASA investigators⁶ enabled the use of these data to generate elevations of non-ocean surfaces such as ice sheets⁷ and later land areas.⁸ Topographic elevations of southern Greenland estimated from both SEASAT and GEOSAT measurements were provided by NASA.

Satellite radar altimeters measure range between the orbit and a reflecting surface by transmitting a signal pulse and timing the delay before the reflected pulse is received. Successful range measurement depends on accurate onboard prediction of the arrival time of the reflected pulse. If the reflected pulse arrives within the predicted window, tracking is maintained and onboard range estimates are made. These ranges are telemetered to the surface along with the total reflected waveform and other information. When the reflected pulse arrives outside the predicted window, loss of track occurs and no range estimates are formed. Over smooth reflecting surfaces, such as the ocean, the reflected pulse assumes a relatively simple waveform and range estimates made onboard are accurate. Over rougher surfaces, such as glacial ice, the waveform of the reflected pulse is more complex and gross errors in the onboard estimates of range can occur. It is possible to make better estimates of range over rougher surfaces by reprocessing the telemetered waveform. This reprocessing is called retracking.⁹

Retracking a telemetered waveform involves fitting it iteratively with either a five-parameter or nine-parameter function, depending on the shape of the waveform. Not all telemetered waveforms can be retracked however, and those that cannot be retracked are edited. After retracking and editing, corrections are applied to the ranges for time tag biases, signal travel time, altimeter antenna offset, ionospheric and tropospheric propagation effects, and solid Earth tide variations. In addition,

satellite orbit corrections, primarily in the radial direction, and a correction for a sloping reflecting surface¹⁰ are also applied. These corrected ranges are used to construct elevations of the reflecting surface.

Over Greenland, because of the uneven distribution of range data over the ice sheet, regular grids of elevations have been developed.^{11,12} Tangent polar stereographic projection grids have been generated so that equal spacing between grid points occurs on the projection plane tangent at the North Pole. A biquadratic or bilinear function describing the surface near a grid point was fit to nearby data. Each altimeter range was assigned an observation standard deviation of 1.0 m. After weighting each observation by the inverse of distance to a desired grid point, a least-squares adjustment was made so that data closest to the grid point influence most of its estimated elevation. The standard deviation of a grid point elevation is a function of how well the elevation represents the data.

The SEASAT spacecraft was launched in late June 1978 and during its brief 110-day lifetime collected radar altimetry data between the latitudes 72° S and 72° N. Investigators at NASA retracked data collected over southern Greenland and used these altimeter ranges to generate a regular grid of surface elevations.¹² Approximately 100,000 data points were used to generate a tangent polar stereographic grid with spacing between grid points of 20 km. Figure 1* shows the geographic pattern from that grid, which extends over the ice sheet, and exposed land of some coastal areas. The grid elevations were referenced to the GEM 10-B geoid. SEASAT-derived elevations may be lower on average than elevations derived by other means from between 2 to 3 m.¹³

The GEOSAT spacecraft was launched in March 1985 and provided 18 months of high-resolution radar altimeter data between latitudes 72° S and 72° N during its primary Geodetic Mission.¹⁴ Eighteen months of data over Greenland were retracked¹¹ and used to generate two grids. Figure 2 shows the geographic pattern from the polar stereographic grid with spacing between points of 20 km. Because GEOSAT provided as much as 10 times the amount of data as SEASAT over the ice sheet (personal communication with Brenner, 1991), NASA also generated a polar stereographic grid with a 10-km spacing between points. The elevations in both grids were referenced to the GEM-10B geoid.

The quality and quantity of non-ocean measurements from the two altimeter missions differ because of hardware and software modifications to GEOSAT.¹⁵ Over the ice sheet, GEOSAT provided denser coverage than SEASAT. Over smaller scale roughness on the ice sheet, GEOSAT tracked better because of modifications to its tracking algorithm. However, because of instrument modifications, once GEOSAT lost track signal reacquisition was not as quick as for SEASAT. For this reason, over ice-free rougher terrain where tracking loss often occurred, SEASAT provided a better description of the topography.

*All figures are presented at the end of the text.

RADIO ECHO SOUNDINGS

During 5 years in the 1970's, 1971-1972,¹⁶ 1974,¹⁷ 1978,¹⁸ and 1979,¹⁹ Danish investigators collected radio echo soundings over an extensive area of Greenland. The data were collected at altitude by aircraft, and Figure 3 shows the tracks of data available from the World Data Center-A for Glaciology [Snow and Ice]. Nearly 26,000 ice surface heights and nearly 18,000 underlying bedrock surface heights were available for southern Greenland. All heights are relative to mean sea level as measured by a barometric altimeter. Figure 4 presents an example of 800 nmi of radio echo soundings collected in 1974 between 68° and 74° N. In this figure the ice surface occasionally reaches more than 2800 m above the bedrock surface.

The principle of a radio-echo sounder is described by Evans and Smith.²⁰ Distances between the instrument and reflecting surface are measured by transmitting a radar pulse and timing the delay before the reflected pulse is received. Measuring distances to the ice and ice-covered bedrock surfaces requires two signals of different frequencies. The higher frequency, 300 MHz, is reflected by the ice surface while the lower frequency, 60 MHz, penetrates the ice and is reflected by the bedrock. During data collection, oscilloscope images of the reflected signals are recorded on 35mm film for later analysis.

The images on the film give a measure of the time elapsed between signal transmission and echo return subject to propagation variations and systematic errors. For all bedrock soundings, the electromagnetic wave velocity of 169 m/ μ s in solid ice with a density of 920 kg/m³ was assumed. Though wave velocity varies with ice density, no corrections were made because the density profile of the ice sheet is generally unknown because of the limited distribution of ice cores.^{21,22} In addition, the broad radiation pattern of the antenna may result in reflections from surfaces not directly below the antenna. Landforms, such as mountains, or inhomogeneities in the ice sheet, such as ice lenses in the firn, far away from the aircraft, may appear on the sounder. Though this phenomenon may add noise to measurements, no corrections were made. Ranges were corrected for the cable length between the transmitter and the antenna because transmission time was measured from the transmitter. The resulting range accuracy of the radar is 10 m or 1 percent of the measured depth, whichever is greater.²⁰ After computing ranges, the positions of the aircraft were used to determine mean sea level elevations.

Associated with each measurement are coordinates determined by an Inertial Navigation System (INS) onboard the aircraft. Coordinates determined by the three-axis INS have a horizontal accuracy of 1-5 km.²³ Inaccuracies in aircraft altitude were large and required correction. Locations defined by the Navy Navigation Satellite System (NNSS) and other sources provided reference points to calibrate track altitudes. Crossovers with calibrated tracks were used to correct those tracks not passing over reference points. Additional comments on the vertical accuracy of the aircraft positions are provided below.

GEOLOGICAL MAP

A tectonic/geological map of Greenland,²⁴ developed by the Geological Survey of Greenland, was obtained through the Library of Congress. Of interest on this map are contours of topographic heights of the ice sheet and exposed land near the coast. Also contoured is the surface underlying the ice. The sources of this topographic information were maps from the Geodætisk Institut, Kobenhaven, and World Aeronautical Charts published by the U. S. Air Force.

GRAVITY ANOMALIES

Gravity measurements collected near the Greenland coast by surface ship and overland by various means were compiled by NRL and the Defense Mapping Agency Aerospace Center (DMAAC). Many sources contributed to these data, but the primary sources were from Greenland, Denmark, the United States, Canada, and Sweden. The distribution of data compiled by NRL is shown in Figure 5 and by DMAAC in Figure 6. As can be seen from these two figures, significant overlap exists between the overland data held by these two organizations. Further, it is evident that an abundance of offshore data exists. These data are primarily sea surface measurements with an occasional sounding. Data on land are concentrated sporadically near the coast with four notable ice-traversing tracks. In both data sets, one track appears near 75° N with two more, nearly overlapping tracks around 70° N. In the DMAAC data set a short 45-km track near 67° N also appears. The overland track data were collected by an aircraft landing on the ice. The data consist of the observation station coordinates and elevation, observed gravity, and free-air and/or Bouguer anomaly.

The gravity anomaly describes perturbations of the field caused by variations in mass distribution. It is the difference between observed gravity reduced to the geoid and a theoretical value on the reference ellipsoid. The *international gravity formula*²⁵ predicts the value of gravity on the ellipsoid as a function of latitude. Various corrections are introduced to reduce the observed value to the geoid. The free-air correction adds to the observed value the effect of the elevation of the observation station. The Bouguer correction is introduced to account for the masses between the station and sea level. The purpose for the gravity reduction defines the type of corrections that are applied to the observed gravity value. In the analysis presented below, free-air anomalies were used because of their strong correlation with topography.

METHODS

Using these data sets, surface elevation grids of the ice and bedrock topography of southern Greenland were developed. The grids were used to model the geopotential of the same area.

SURFACE ELEVATION GRIDS

Independently no single data set sufficiently describes either the ice or bedrock surface. For this reason, composite data sets for the ice surface and bedrock surface were developed. This involved editing data sets based on their relative strengths and merging them. After the composite data sets were developed, they were interpolated into rectangular grids.

The topographic elevations of Greenland south of 72° N, including the inland ice sheet and coastal ice-free areas, will be referenced as the *composite ice surface*. The composite ice surface was developed from three data sources. The GEOSAT 20-km elevation grid provided data for the interior ice sheet, which were consistent with large-scale features found on the geological map. Further, comparisons of these data with the SEASAT 20-km grid elevations²⁶ indicated a significant average height increase, which is consistent with a growing ice sheet. However, in coastal ice-free land areas defined by Bindschadler's maps,¹³ the GEOSAT 20-km grid contained sporadic negative elevations. These were inconsistent with elevation contours on the geological map and different from the SEASAT 20-km grid elevations* by as much as 1.99 km. For these reasons, the GEOSAT negative elevations were manually edited and replaced with SEASAT or other elevation data (Figure 7). SEASAT elevations were substituted when consistent with the geological map and when SEASAT grid point uncertainties were significantly smaller than those from GEOSAT. In locations where neither GEOSAT nor SEASAT provided reliable data, elevations were estimated using averages of nearby elevations from the NRL gravity data base. The remaining negative heights, principally near the coast, were substituted with values interpolated between the ocean surface and valid data base grid points above sea level.

The elevations of ice-covered bedrock and coastal ice-free areas south of 72° N will be referenced as the *composite bedrock surface*. The composite bedrock surface was developed from the Danish radio echo soundings of the bedrock and other data. In the coastal ice-free areas where gaps exist in the radio echo soundings, the Danish data were supplemented with the manually edited elevations from the composite ice surface data base, their locations shown in Figure 7. These data were used to generate the composite bedrock surface elevation grid.

* In the coastal areas where terrain is rougher than over the inland ice, SEASAT generally described the topography better than GEOSAT (see the Satellite Radar Altimetry section).

In addition to the composite ice surface elevation grid developed primarily with satellite altimetry, a second grid of that surface was generated. Using the Danish soundings of the ice surface and the same manually edited elevations supplementing the bedrock elevations, the Danish ice surface elevation grid was generated.

All three surface elevation grids were developed from their source data in a similar manner. Each respective data set was augmented with zeros representing ocean surface elevations. These zeros extended outward from the shoreline, making the dimensions of the rectangular grid area 38.4 longitude degrees by 12.0 latitude degrees. Using these augmented data sets, grids with a spacing between grid points of 0.2 deg in latitude and longitude were developed.

A technique developed by Braile²⁷ was used to interpolate the data onto a regular rectangular grid. This technique is based on fitting a polynomial to a small region of the grid area. The fitting region contains several grid points and is moved successively as a template over the entire grid area. The characteristics of the gridding operation can be controlled by the choices of the order of the polynomial, the size of the fitting region, and the number of grid points to interpolate in each fit region. The best-fitting, in a least-squares sense, surface is determined and from it grid points are interpolated.

The order of the polynomial used is dependent on the number of data points in the fitting region. The chosen order of the polynomial is reduced dynamically until the number of points available are sufficient for solution. This provides for optimum fitting in areas of high and low data density and minimizes edge effects. The grids of all three surfaces were made using a third-order polynomial. The fit region template for the ice surface grid was 2 deg square while those of the bedrock and Danish ice surface grids were 3 deg square. Larger fitting regions were used for the latter two surfaces because of track-spacing irregularity and gaps in data distribution. Sixteen grid points were interpolated per fit region for all three surfaces.

The first two of these grids were subsequently used to generate a model of the geopotential trends in southern Greenland. The third grid, the Danish ice surface, was used to evaluate the elevation accuracy of the bedrock surface where defined by the radio echo sounding data.

GEOPOTENTIAL MODELING

The *composite topographic data base* of southern Greenland consists of mean sea level elevations of the ice surface and bedrock surface in grids with a spacing between points of 0.2 deg. This data base provides, assuming a density structure, the localized mass distribution and thus insight into geopotential components. As constructed from available source data, the elevation grids cover the area between 60.5° and 72.3° N latitude and between 20.8° and 59.0° W longitude. There are 11520 data base elements each having two elevation values. Elements located offshore had zero

elevations before the gridding procedure; however, because of edge effects of the surface fit, small nonzero elevations exist in some locations near shore. For inland elements, the lower elevations define either the exposed bedrock surface or the interface between the bedrock and overlying ice. The upper elevations, when different, provide the surface topography of the Greenland ice sheet. Thus, the composite topographic data base defines the mass distribution for southern Greenland as two sets of rectangular prisms with common element bases, see Figure 8.

The geopotential effect of this irregular mass distribution can then be calculated at discrete points. Assuming a constant density for the material within each prism element, the data base becomes a finite element representation for the mass distribution. Taking 2.67 g/cm^3 as the density of the bedrock layer and 1.00 g/cm^3 ⁴ for the ice layer, two integrations over the mass layers are required to calculate the effect of the masses at a given point.

The numerical integration is accomplished using the methods described in Forsberg,²⁸ which provides closed-form expressions for the contribution of individual elements (rectangular prisms) to various gravimetric quantities. At each computation point, these formulas are evaluated then summed over all elements of the composite data base, implying up to 23040 computations for each point, since two distinct density layers are present. In practice, templates of desired radii may be used to reduce the complexity of the computations. An inner template defines the region where exact formulas are used. A larger template zone is defined in which approximations are made to increase computation speed. Prisms external to the second template radius are processed with still further approximations. The template radii for the computations performed in this study were 50 and 1000 km.

The result of this integration is the components of various gravimetric quantities due to the anomalous mass distribution above mean sea level. These components are wavelength limited by the resolution of the data base and represent only part of the amplitude of the full geopotential field. The results of modeling only the anomalous mass distribution, if accurate, should correlate with intermediate wavelengths of the full geopotential field and provide insight into geopotential trends in the region. Geopotential forecasts based on this model are compared with free-air anomaly profiles below.

⁴ 1.00 g/cm^3 was used in all calculations involving the ice sheet. Although the density of ice at 0°C is 0.92 g/cm^3 , the temperature and pressure distribution throughout the Greenland ice sheet is complicated and unknown. Given the resolution and accuracy of the data base, the assumed density was considered sufficient for the purpose of this analysis.

RESULTS

COMPOSITE TOPOGRAPHIC DATA BASE

The contoured ice surface presented in Figure 9, and its three-dimensional perspective in Figure 10, show features similar to those generated by NASA investigators.^{11,13} The highest elevations, over 3100 m, occur near the northern extent of the area. An ice ridge strikes NNE through the center of the ice sheet flanked by steep gradients on the east coast and more gentle gradients on the west.

The contoured bedrock surface presented in Figure 11, and its three-dimensional perspective in Figure 12, show physiographic features consistent with, but in much more detail than, the geological map. Apparent on the east coast are the steep gradients of mountain ranges formed by uplifted Paleozoic folds. In the center of the island, the southern northward-tilting basement block may be evidenced by the slope in that direction. The depression, possibly separating the two tilted basement blocks, can be seen between 68° N and 70° N.

The contoured Danish ice surface presented in Figure 13 has features similar to the ice surface in Figure 9. The mean elevation difference* between these two surfaces is -12 m with a sigma of 170 m. The sign of this result indicates that the composite ice surface is on the average slightly higher than the Danish ice surface. Figure 14 gives the locations of differences whose absolute values were greater than 100 m. These differences are primarily located in the coastal regions, where gaps in the Danish soundings exist, and near the northern limit of the map area where grid edge effects may introduce variability. Although differences between these two surfaces exist, the Danish ice surface is generally consistent with the composite ice surface. This is evidence that the vertical positions of the aircraft collecting these data were well determined, and the Danish ice surface soundings are an accurate data set. Further, the Danish bedrock surface soundings, collected simultaneously with the ice surface soundings and reduced in a similar manner, have acceptable vertical control. This suggests that the composite bedrock surface is generally an accurate description of the physical bedrock surface where data are available.

GRAVITY DISTURBANCE AND VERTICAL DEFLECTION TRENDS IN SOUTHERN GREENLAND

With assumed values for the density of the ice and bedrock layers, the topographic data base was used to approximate the mass distribution of southern

* Only differences whose absolute values were greater than 0.05 m were used to determine these statistics, thus eliminating ocean grid points with null elevations.

Greenland. The geopotential effect of this irregular mass distribution was then calculated for discrete points lying external to the mass. The quantities determined through these computations were gravity disturbance and vertical deflection.

Since the survey of Greenland is planned to be flown at constant altitude, geopotential computations for southern Greenland were made on a constant altitude surface 2000 ft above the highest grid point in the data base (3195 m). The computed values of gravity disturbance and vertical deflection, at a grid spacing equivalent to that of the data base, were contoured. The results are provided in Figure 15 for gravity disturbance and in Figures 16 and 17 for the two components of vertical deflection. The gravity disturbances at altitude provide insight into the spatial wavelengths of the field and thus can contribute to the airborne survey design. For example, in the central longitude zones of the island, where the ice sheet is the dominate feature, the geopotential field is more slowly varying. To the resolution and accuracy of the data base, there are east-west variations as small as 70 mgal over distances as great as 15 deg. Contrasted to this are the coastal zones, which demonstrate variations in gravity disturbance of up to 200 mgal over 2.5-deg arc lengths, with even higher gradients in some regions. These high-amplitude spatial variations are associated with the large variations in the bedrock topography in many coastal areas (see for instance Figure 11). These larger gradients are also found in the east-west component of vertical deflection along the eastern coastal regions as shown in Figure 17.

A three-dimensional perspective of the disturbances at altitude is given by Figure 18. Notice that the disturbance field is highly correlated with the bedrock topography (Figure 12) as expected.

In terms of survey design for geopotential recovery, these results suggest that denser spaced tracks are required in an east-west direction in many coastal regions with greater track spacing being adequate over most of the central ice sheet. Without the use of a track-spacing factor that is geographically adjusted, it is likely that the mean gravity anomalies recovered from the airborne data will demonstrate significant biases in these high gradient provinces.

In the section that follows, examples of gravity disturbances on the surface computed from the topographic model will be compared with measured free-air anomalies.

COMPARISON OF GEOPOTENTIAL FORECASTS WITH FREE-AIR ANOMALY DATA

Linear Profiles

The gravity disturbance on the physical surface P' is related to the free-air gravity anomaly to first order by the following equation:

$$\delta g_{P'} = \Delta g_P + \left(\frac{\partial g}{\partial h} - \frac{\partial \gamma}{\partial h} \right) H - \frac{\partial \gamma}{\partial h} N \quad (1)$$

where P is the corresponding point on the geoid; H is orthometric height; N is the undulation at P and γ is normal gravity. Examining the contribution of each term in the right-hand side of Equation 1, it is evident that the gravity disturbance will be spatially correlated with free-air anomaly.

In the comparisons that follow, that part of the total gravity disturbance of Equation 1 due to the anomalous mass distribution above mean sea level is computed from the composite topographic data base at the surface locations P' where point anomaly data have been measured. Since this component of the total disturbance is due to the anomalous mass, it is expected to also demonstrate a strong correlation with topography and thus with the free-air anomaly, again to the resolution and accuracy of the data base.

Figure 19 shows the location of a primarily east-west anomaly profile across southern Greenland found in the NRL holdings. The profile has a longitude extent of over 16 deg. Using the data base model, gravity disturbances were computed at the locations of these surface gravity stations. The location of each point was extracted from the NRL gravity anomaly file along with the point elevation. Figure 20 provides the free-air anomaly values along the profile and the gravity disturbances simulated from the data base model. The disturbances here have been translated by the subtraction of 93.1 mgal to bring the two scales into general agreement. A comparison of these profiles shows that the overall trend in the actual anomaly data appears in the simulated results. Several of the shorter wavelength variations are common to both profiles although the variation in magnitude of the simulated data is much less.

Figure 21 gives the location of another free-air anomaly profile found in the data provided by DMAAC. This profile covers approximately 2.5 deg of longitude near the eastern coast. The disturbances at these locations predicted by the topographic model, translated by -79.7 mgal, are found in Figure 22 along with the anomaly data. Again the overall decreasing trend in the free-air data is present in the disturbance profile.

Figure 23 shows a companion profile from the NRL data set to the profile in Figure 19, with approximately 15 deg extent in longitude. Figure 24 provides the free-air anomaly and computed disturbance profiles after removal of 83.0 mgal. In this example, the general trend over the extent of the track is present in the disturbance results; however, its slope is significantly greater than in the anomaly data. Shorter wavelengths seen in the anomaly data are generally missing from the disturbance.

Two points need to be made regarding these results. First, using the topographic data base and constant layer density, intermediate wavelength trends in the observed anomaly data can generally but not always be predicted. Because of the resolution and accuracy of the data base and density assumptions, short wavelengths in the field are generally not represented by the model. The shortest wavelengths that can be represented are about 0.4 deg. Thus, the computed disturbance field is generally smoother than what will be acquired by the airborne survey. Second, since the disturbances are based solely on the modeled representation of anomalous mass above mean sea level, all numerical results will be biased due to the geopotential of unmodeled mass below mean sea level.

Area Profiles

To further evaluate the model, three-dimensional perspectives of observed free-air anomalies and computed gravity disturbances were generated. The observations, collected on the surface in several regions near the coast, are irregularly distributed and contain gaps. The gravity disturbances were computed at the same locations where observations were collected. Before perspectives were generated, regular grids were developed during which values were interpolated in areas void of data. Therefore, the features in these areas, shaded in the figures, are probably inaccurate and should be ignored. The coastal regions presented often coincide with areas where data base elevations are weakest and where extensive data editing was necessary. For these reasons, some disagreement is expected in the comparisons between perspectives of the computed gravity disturbances and those produced from measured gravity anomalies.

The first area considered, known as Gåsefjord, is shown in Figure 25. Twenty-five measured free-air anomalies in the area were found in the gravity data provided by NRL. An enlargement of the area showing the locations of the free-air anomalies is given in Figure 26. Figure 27 shows the three-dimensional perspective of these anomalies and the computed gravity disturbances. In the rectangular area presented, there is no occurrence of measured anomalies (see Figure 26) in the southwest corner so the corresponding area is shaded in Figure 27. A comparison of the light surfaces shows some common trends. For instance, each surface shows a dominant crest extending west from near 69.5° N. On the southwest side near 27° W, a smaller convex feature appears on both surfaces.

Figure 28 provides the value of the free-air anomaly and disturbance at each of the 25 points of Figure 26 numbered consecutively from west to east. Of the 24 consecutive pairs of points in this ordering scheme, the direction (increase or decrease) of change in the anomaly was predicted using the model disturbances in 22 cases. Success in predicting the magnitude of the change varied.

A second example is provided by the anomaly data available in Holsteinsborg, Figures 29 and 30. The three-dimensional perspective of the anomaly data and

modeled disturbance appear in Figure 31. Again trends in the anomaly data are predictable using the modeled disturbances. For example, a prominent eastward slope appears in the anomalies and the disturbances.

A third example of this type of comparison is Jameson Land, Figures 32, 33, and 34.

CONCLUSIONS

Regular grids of the ice surface and bedrock surface of southern Greenland with assumed density structures provide models of the localized mass distribution and insight into intermediate wavelengths of the geopotential. The geopotential model is limited by the resolution and accuracy of the composite topographic data base and the assumption of density homogeneity in the ice and bedrock layers. Track and regional comparisons between the modeled geopotential and free-air anomaly data collected on the island generally show similarities in their intermediate wavelengths. Though short wavelengths of the anomalous field are not represented in the model, it can support survey design and interpretation of new survey data from the region. Further comparisons of the model with data acquired in 1991 are planned.

REFERENCES

1. Erozena, J. M., M. F. Peters, M. J. Chalona, and G. L. Mader, "The Greenland Aerogeophysics Project," *EOS, Transactions, American Geophysical Union*, Vol. 72, No. 20, p. 232, 14 May 1991.
2. Kim, J., and R. H. Rapp, *The Development of the July 1989 1° x 1° and 30' x 30' Terrestrial Mean Free-Air Anomaly Data Bases*, Report 403, Department of Geodetic Science and Surveying, The Ohio State University, Columbus, Ohio, 98 pages, January, 1990.
3. Haller, J., *Geology of the East Greenland Caledonides*, Interscience Publishers, John Wiley & Sons Ltd., New York, 392 pages, 1971.
4. Ten Brink, N. W., "Glacio-Isostasy: New Data from West Greenland and Geophysical Implications," *Geological Society of America Bulletin*, Vol. 85, No. 2, pp. 219-228, 1974.
5. Bloom, A. R., *Geomorphology*, Prentice-Hall Inc., Englewood Cliffs, New Jersey, 510 pages, 1978.

REFERENCES (CONTINUED)

6. Martin, T. V., H. J. Zwally, A. C. Brenner, and R. A. Bindschadler, "Analysis and Retracking of Continental Ice Sheet Radar Altimeter Waveforms," *Journal of Geophysical Research*, Vol. 88, No C3, pp. 1608-1616, 1983.
7. Zwally, H. J., R. A. Bindschadler, A. C. Brenner, T. V. Martin, and R. H. Thomas, "Surface Elevation Contours of Greenland and Antarctic Ice Sheets," *Journal of Geophysical Research*, Vol. 88, No. C3, pp. 1589-1596, 1983.
8. Frey, H., and A. C. Brenner, "Australian Topography from SEASAT Overland Altimetry," *Geophysical Research Letters*, Vol. 17, No. 10, pp. 1533-1536, 1990.
9. Zwally, H. J., A. C. Brenner, J. A. Major, T. V. Martin, and R. A. Bindschadler, "Satellite Radar Altimetry Over Ice," *NASA Reference Publication 1233*, Vol. 1, 145 pages, 1990.
10. Brenner, A. C., R. A. Bindschadler, R. H. Thomas, and H. J. Zwally, "Slope-Induced Errors In Radar Altimetry Over Continental Ice Sheets," *Journal of Geophysical Research*, Vol. 88, No. C3, pp. 1617-1623, 1983.
11. Zwally, H.J., J. A. Major, A. C. Brenner, and R. A. Bindschadler, "Ice Measurements by GEOSAT Radar Altimetry," *Johns Hopkins APL Technical Digest*, Vol. 8, No. 2, pp. 251-254, 1987.
12. Zwally, H. J., J. A. Major, A. C. Brenner, R. A. Bindschadler, and T. V. Martin, "Satellite Radar Altimetry Over Ice," *NASA Reference Publication 1233*, Vol. 2, 82 pages, 1990.
13. Bindschadler, R. A., H. J. Zwally, J. A. Major, and A. C. Brenner, "Surface Topography of the Greenland Ice Sheet from Satellite Radar Altimetry," *NASA SP-503*, 103 pages, 1989.
14. McConathy, D. R., and C. C. Kilgus, "The Navy GEOSAT Mission: An Overview," *Johns Hopkins APL Technical Digest*, Vol. 8, No. 2, pp. 170-175, 1987.
15. Brenner, A. C., H. V. Frey, and H. J. Zwally, "Comparisons Between GEOSAT and SEASAT Tracking Over Non-Ocean Surfaces," *Geophysical Research Letters*, Vol. 17, No. 10, pp. 1537-1540, 1990.
16. Overgaard, S., *Radio Echo Sounding In Greenland Data Catalogue 1971/1972*, Electromagnetic Institute, Technical University of Denmark, 71 pages, 1982.
17. Overgaard, S., *Radio Echo Sounding In Greenland Data Catalogue 1974*, Electromagnetic Institute, Technical University of Denmark, 104 pages, 1981.

REFERENCES (CONTINUED)

18. Overgaard, S., *Radio Echo Sounding In Greenland Data Catalogue 1978*, Electromagnetic Institute, Technical University of Denmark, 138 pages, 1984.
19. Overgaard, S., *Radio Echo Sounding In Greenland Data Catalogue 1979*, Electromagnetic Institute, Technical University of Denmark, 175 pages, 1984.
20. Evans, S., and B. M. E. Smith, "A Radio Echo Equipment for Depth Sounding in Polar Ice Sheets," *Journal of Scientific Instruments*, Series 2, Vol. 2, pp. 131-136, 1969.
21. MacKinnon, P. K. (editor), "Ice Cores," *Glaciological Data, Report GD-8*, World Data Center-A for Glaciology [Snow and Ice], Boulder, Colorado, 139 pages, 1980.
22. Brennan, A. M., and R. G. Barry, (editors), "Ice Cores Update 1980-1989 Permafrost Data Workshop," *Glaciological Data, Report GD-23*, World Data Center-A for Glaciology [Snow and Ice], Boulder, Colorado, 127 pages, 1990.
23. Overgaard, S., and N. S. Gundestrup, "Bedrock Topography of the Greenland Ice Sheet in the Dye 3 Area," *Greenland Ice Core: Geophysics, Geochemistry, and the Environment*, Geophysical Monograph 33, American Geophysical Union, pp. 49-56, 1985.
24. Escher, A., N. Henriksen, P. R. Dawes, and A. Weidick, *Tectonic/Geological Map of Greenland*, The Geological Survey of Greenland, Copenhagen, Denmark, 1970.
25. Heiskanen, W. A., and H. Moritz, *Physical Geodesy*, W. H. Freeman and Company, San Francisco, 364 pages, 1967.
26. Zwally, H. J., A. C. Brenner, J. A. Major, R. A. Bindschadler, and J. G. Marsh, "Growth of the Greenland Ice Sheet: Measurement," *Science*, Vol. 246, pp. 1587-1598, 1989.
27. Braile, L. W., "Comparison of Four Random to Grid Methods," *Computers & Geosciences*, Vol. 4, pp. 341-349, 1978.
28. Forsberg, R., *A Study of Terrain Reduction, Density Anomalies and Geophysical Inversion Methods in Gravity Field Modeling*, Report 355, The Department of Geodetic Science and Surveying, The Ohio State University, Columbus, Ohio, 129 pages, April, 1984.

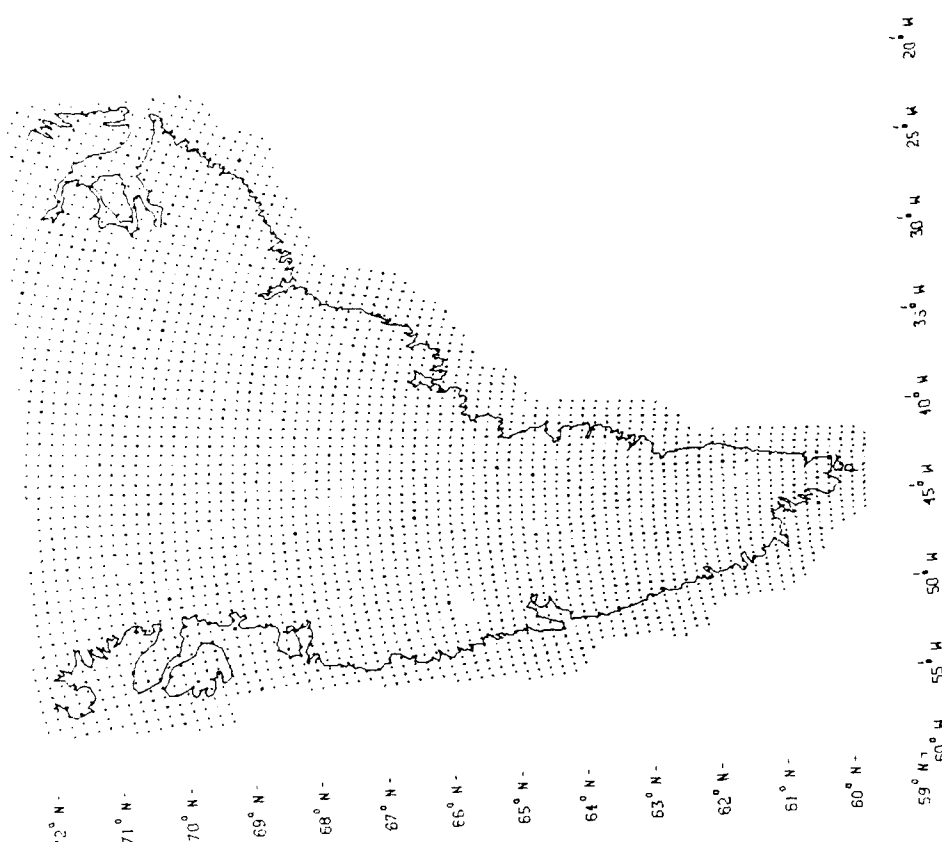


FIGURE 1. GRID OF SURFACE ELEVATIONS DERIVED FROM SEASAT RADAR ALTIMETRY. SPACING OF GRID POINTS IS 20 km ON PROJECTION PLANE AT 90° N.

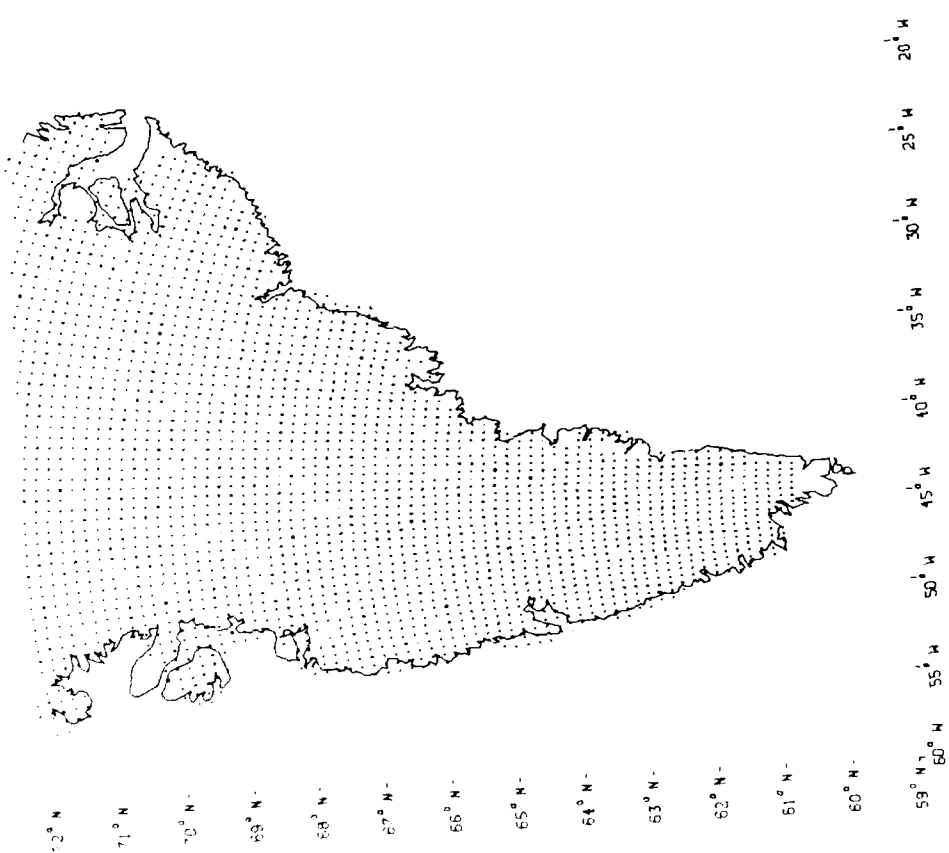


FIGURE 2. GRID OF SURFACE ELEVATIONS DERIVED FROM GEOSAT RADAR ALTIMETRY. SPACING OF GRID POINTS IS 20 km ON PROJECTION PLANE AT 90° N.

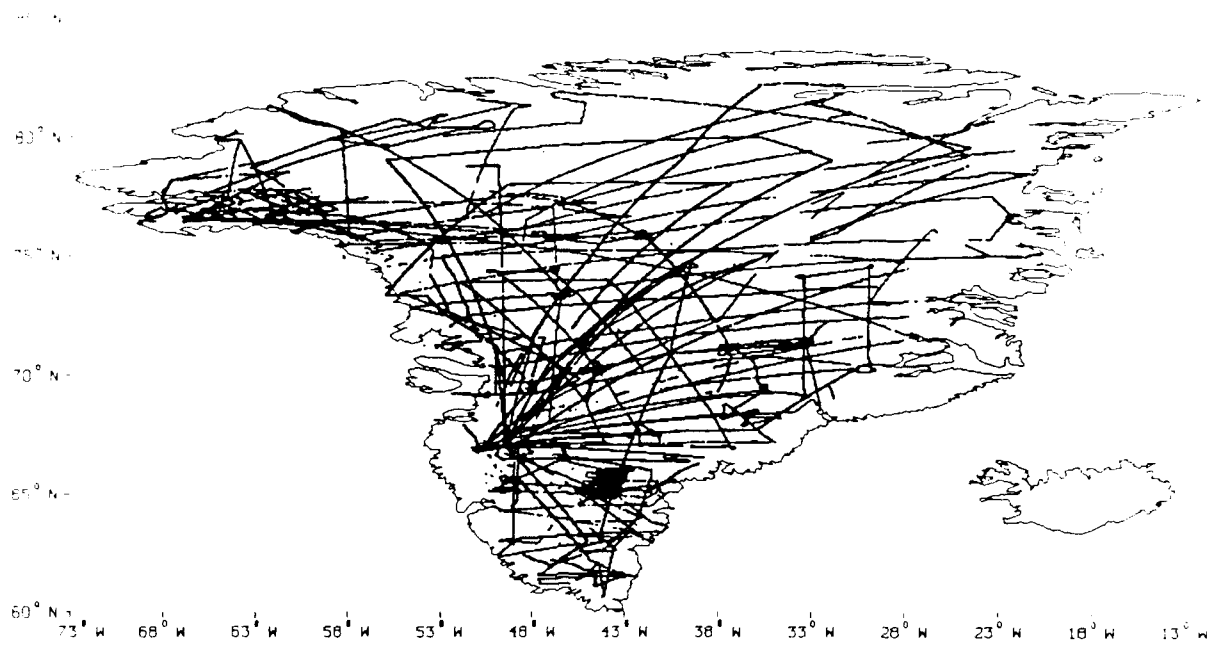


FIGURE 3. TRACK DISTRIBUTION OF DANISH RADIO ECHO SOUNDINGS. SHOWN ARE 5 YEARS OF DATA.

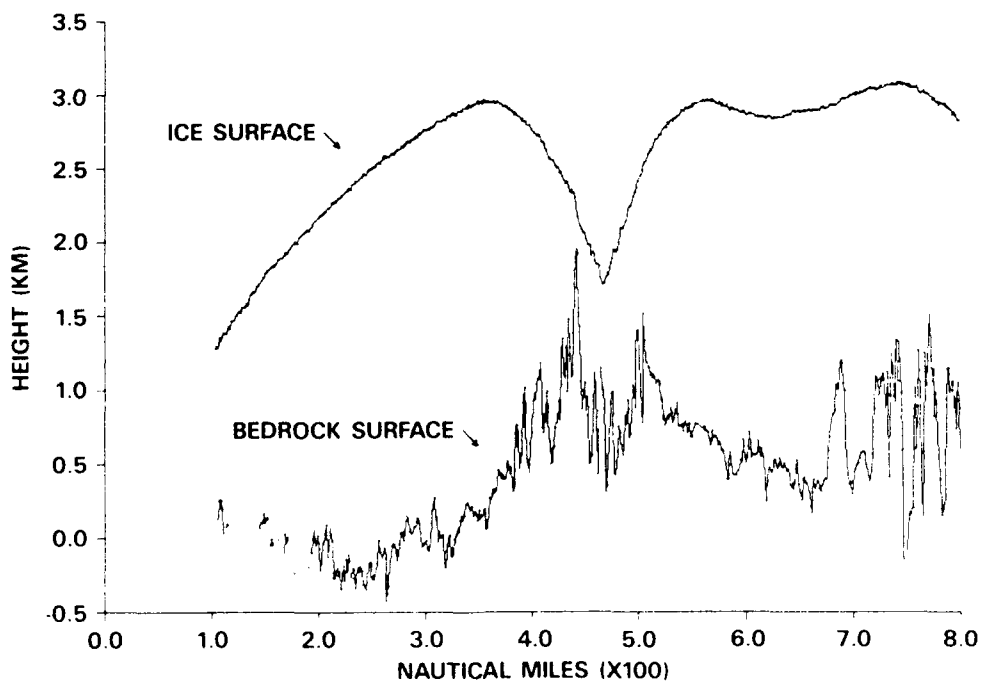


FIGURE 4. EXAMPLE OF DANISH RADIO ECHO SOUNDINGS PROFILE. COLLECTED IN 1974 BETWEEN 68° N AND 74° N.

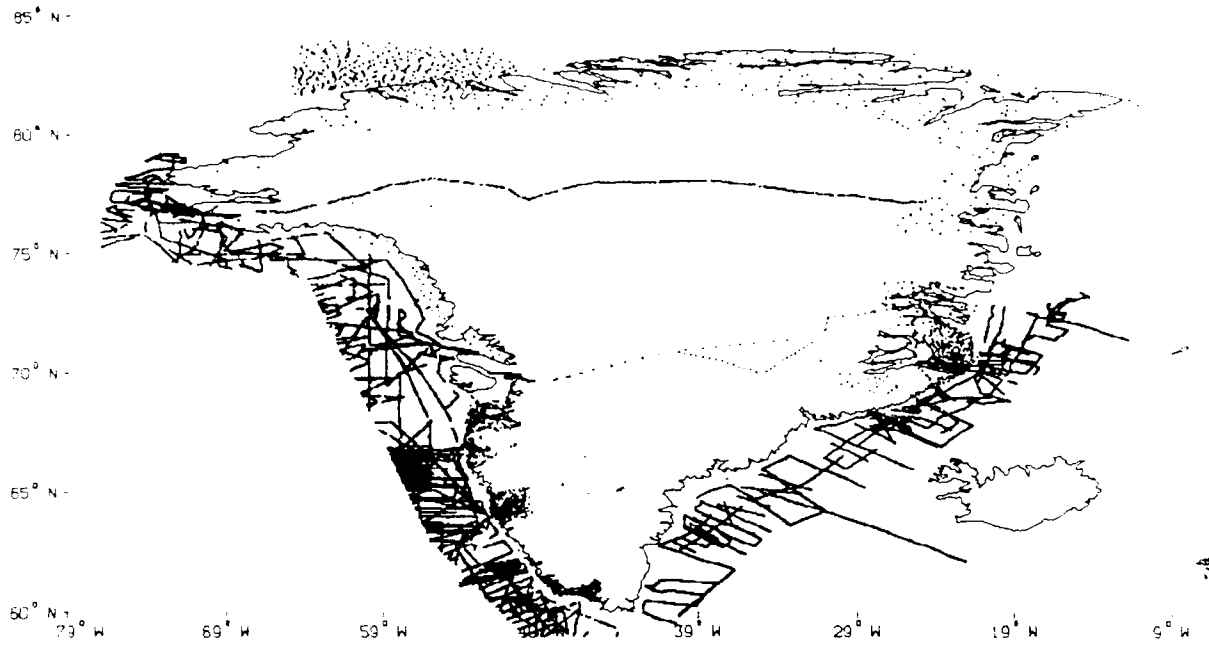


FIGURE 5. NRL GRAVITY ANOMALIES

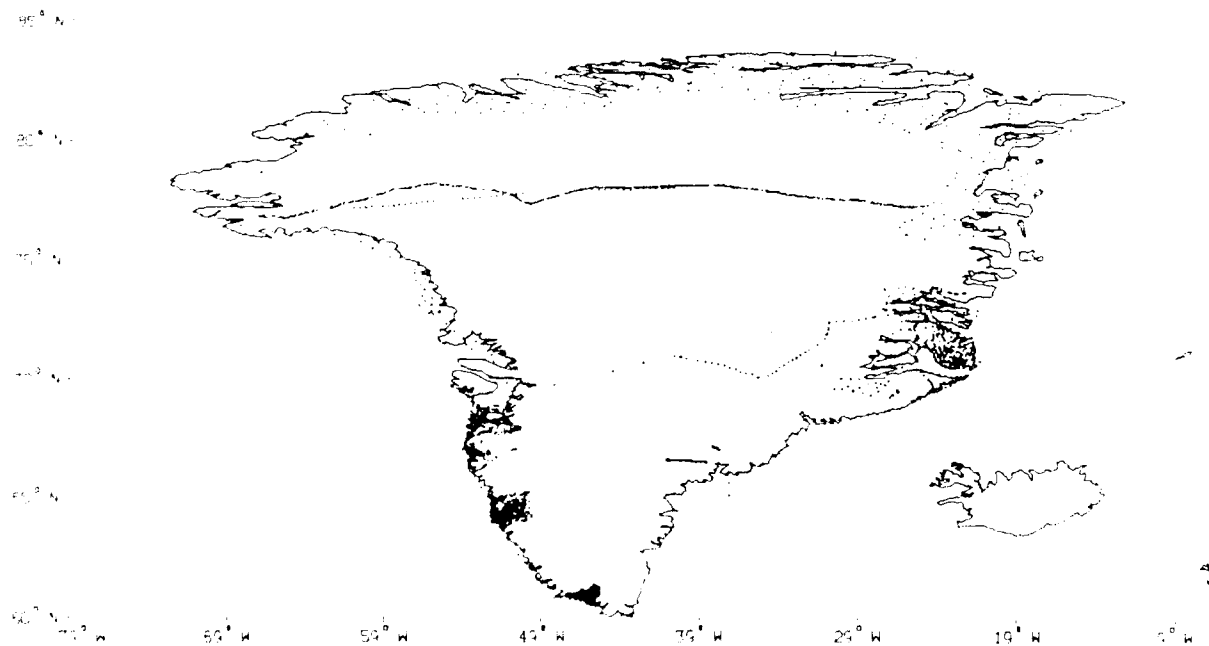


FIGURE 6. DMAAC GRAVITY ANOMALIES

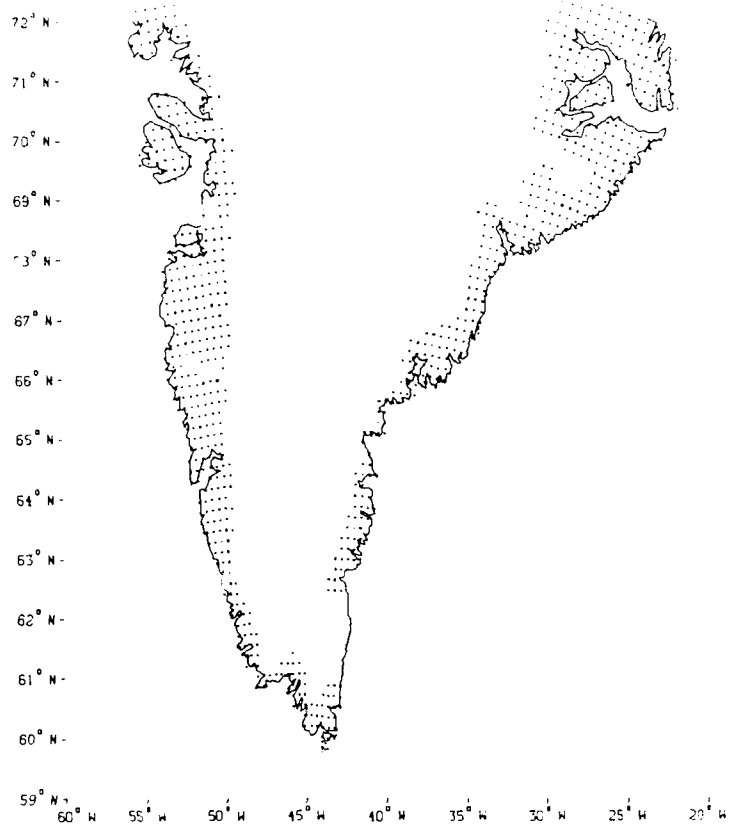


FIGURE 7. LOCATIONS OF MANUALLY EDITED DATA

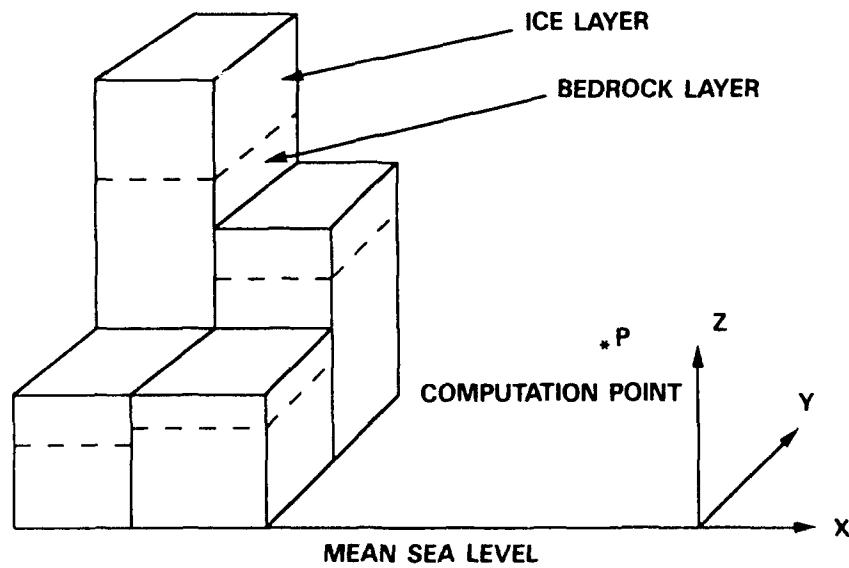


FIGURE 8. DUAL PRISM MODELS WITH COMMON BASES FOR ICE AND BEDROCK MASS DISTRIBUTIONS

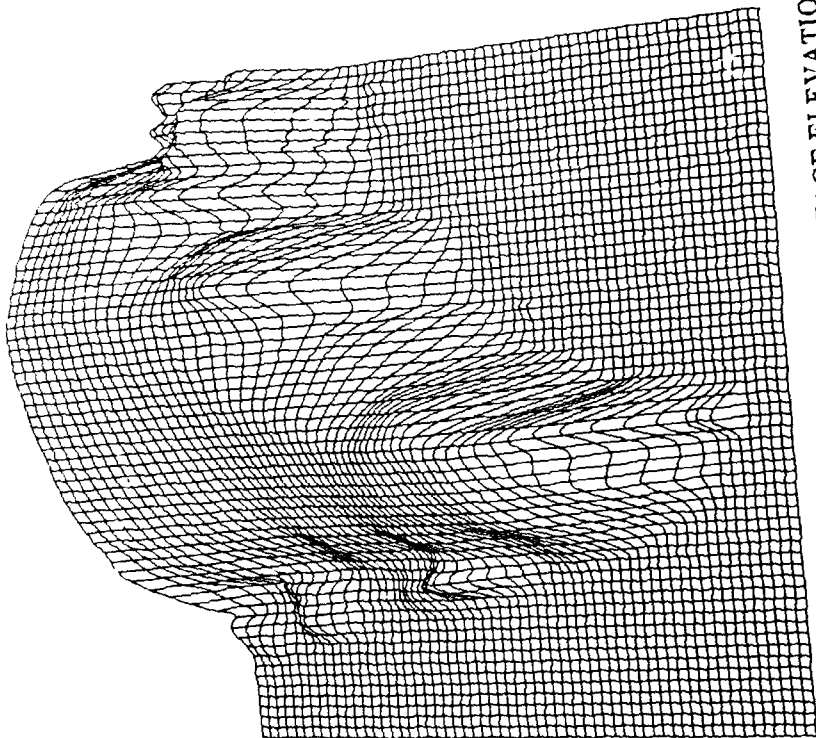


FIGURE 10. 3D PERSPECTIVE OF SURFACE ELEVATIONS OF SOUTHERN GREENLAND. VIEW IS FROM SSW VERTICAL SCALE EXAGGERATED.

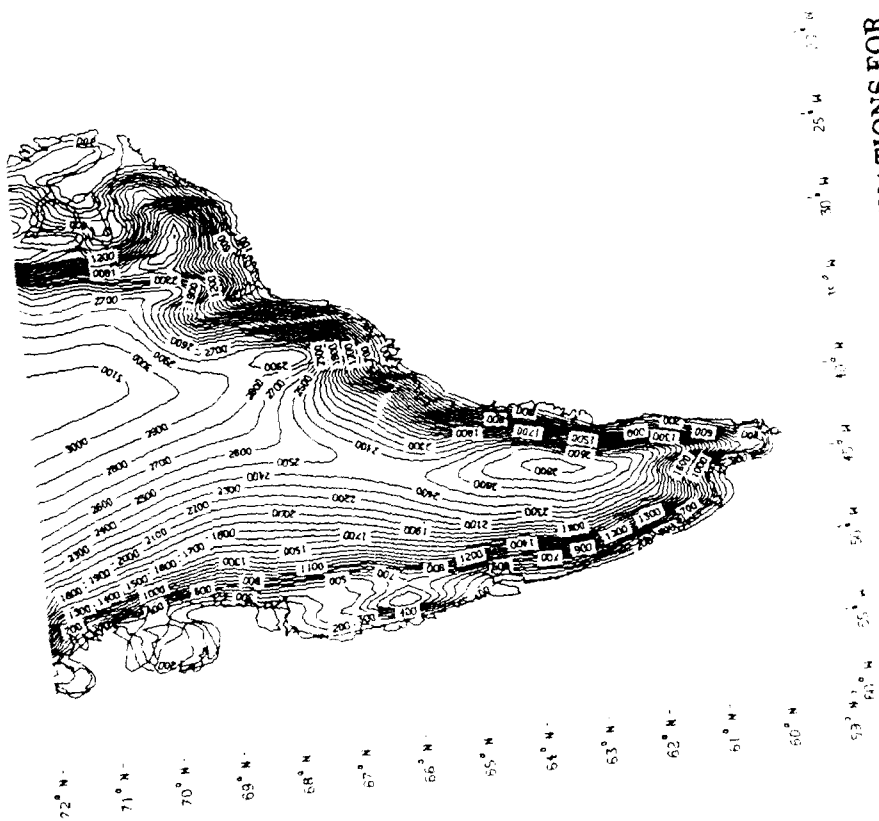


FIGURE 9. CONTOUR OF SURFACE ELEVATIONS FOR SOUTHERN GREENLAND. CONTOUR INTERVAL IS 100 M.

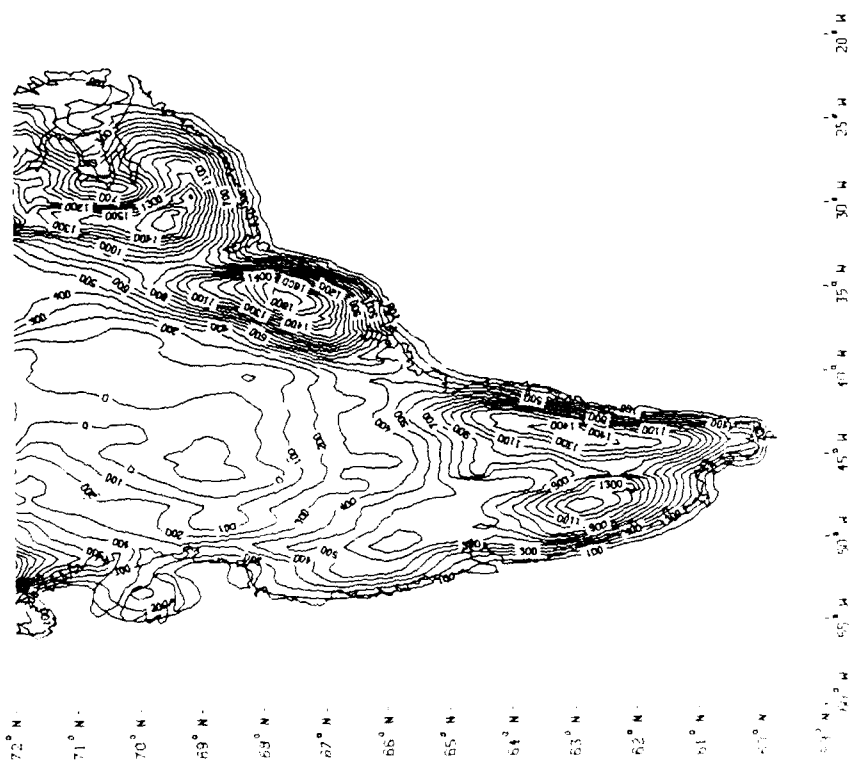


FIGURE 11. CONTOUR OF BEDROCK ELEVATIONS FOR SOUTHERN GREENLAND. CONTOUR INTERVAL IS 100 M.

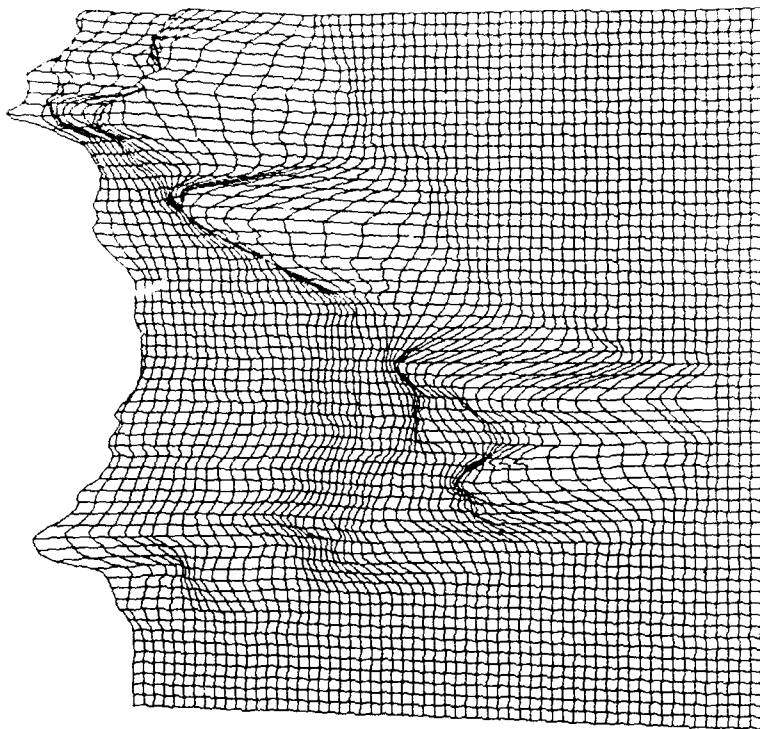


FIGURE 12. 3D PERSPECTIVE OF BEDROCK ELEVATIONS OF SOUTHERN GREENLAND. VIEW IS FROM SSW. VERTICAL SCALE EXAGGERATED.

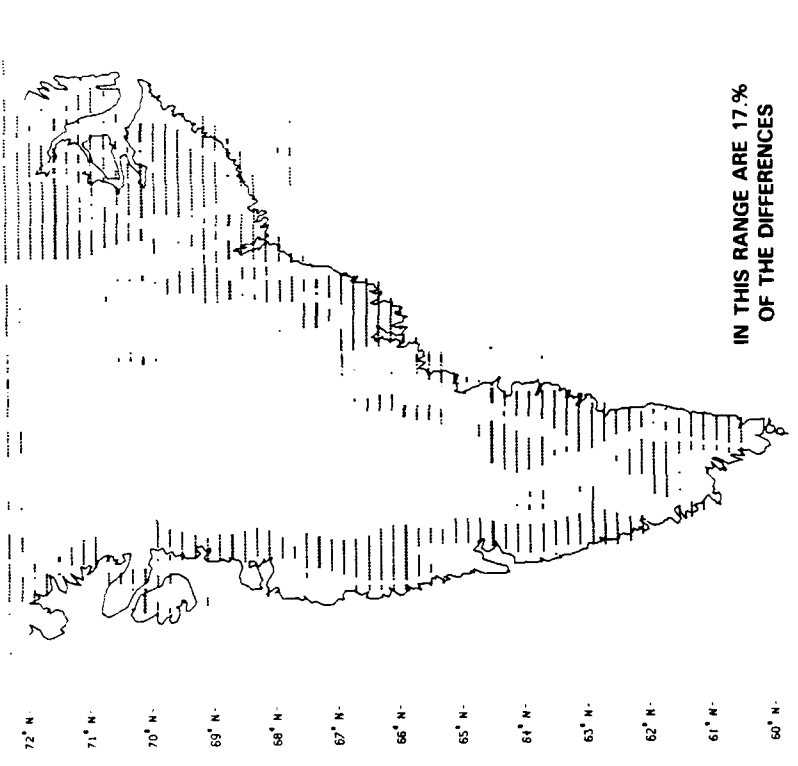


FIGURE 14. COMPARISONS OF ELEVATIONS OF TWO ICE SURFACES: COMPOSITE VS DANISH. PLOTTED ARE THE LOCATIONS OF DIFFERENCES WITH AN ABSOLUTE VALUE GREATER THAN 100 M.

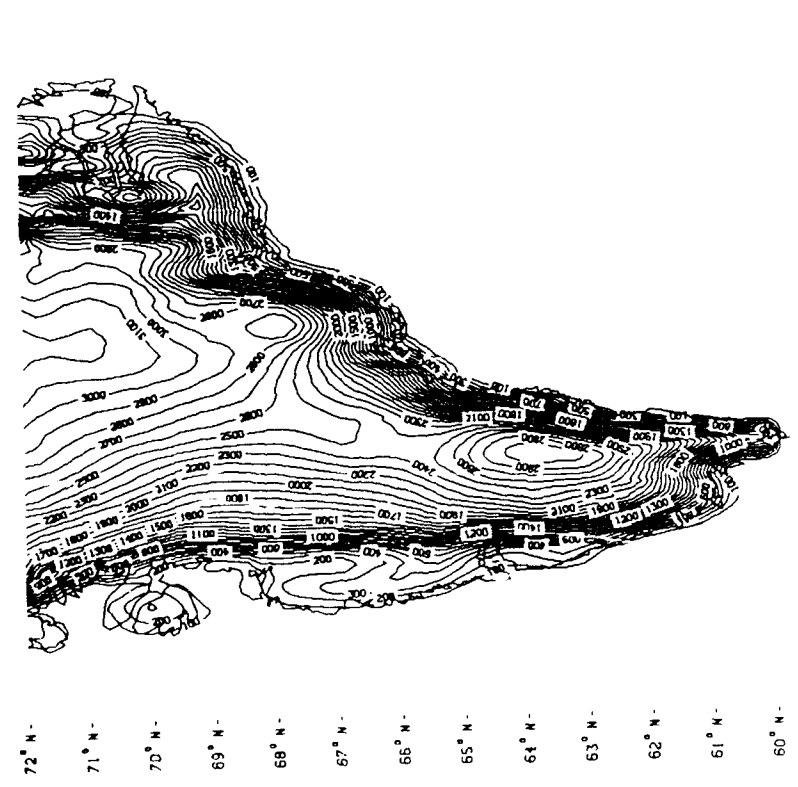


FIGURE 13. CONTOUR OF SURFACE ELEVATIONS BASED ON DANISH SOUNDINGS. CONTOUR INTERVAL IS 100 M.

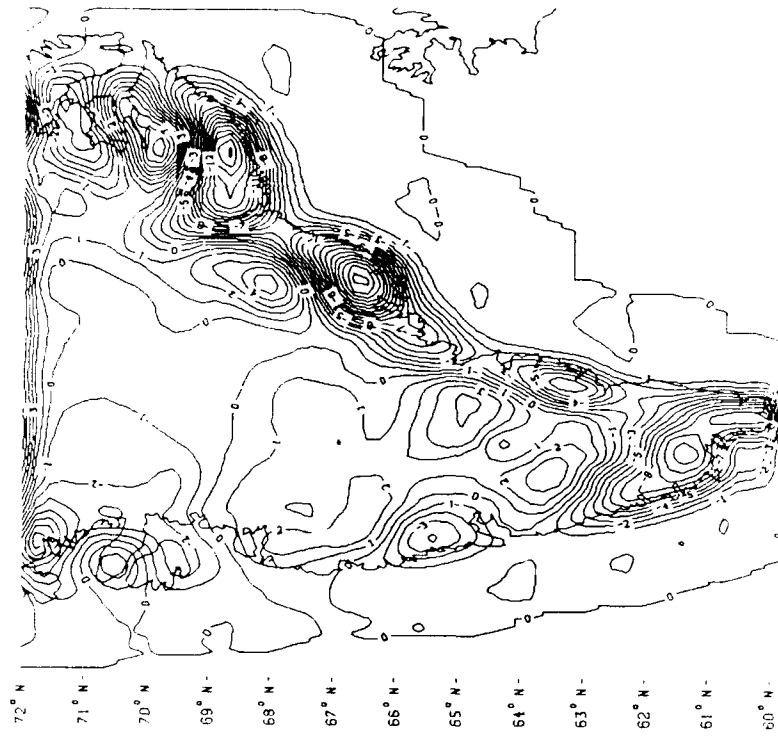


FIGURE 15. GRAVITY DISTURBANCE AT 3800 M
BY TOPOGRAPHIC REDUCTION CONTOUR
INTERVAL IS 10 MGAL.

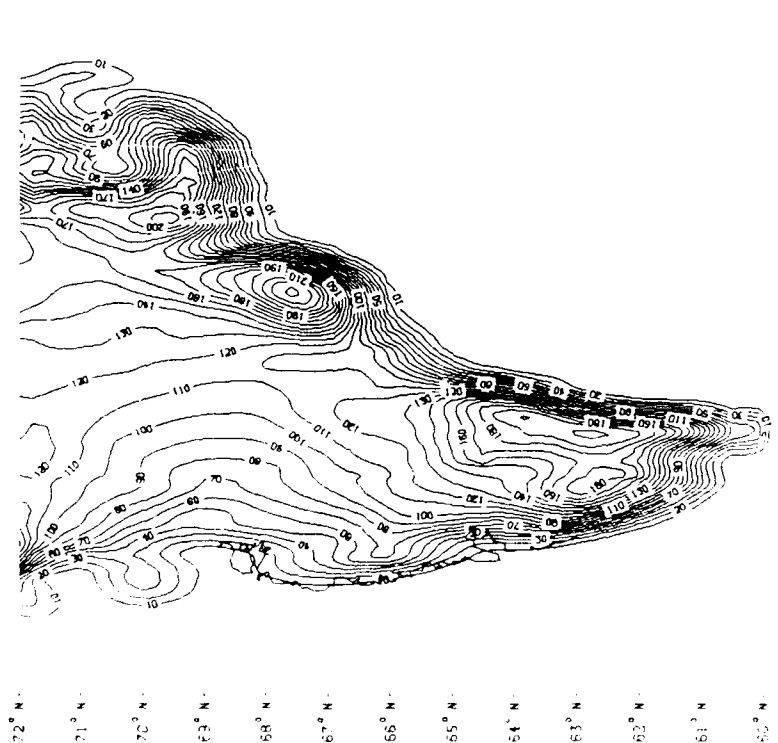


FIGURE 16. VERTICAL DEFLECTION ξ AT 3800 M
BY TOPOGRAPHIC REDUCTION CONTOUR
INTERVAL IS 1 ARCSEC.

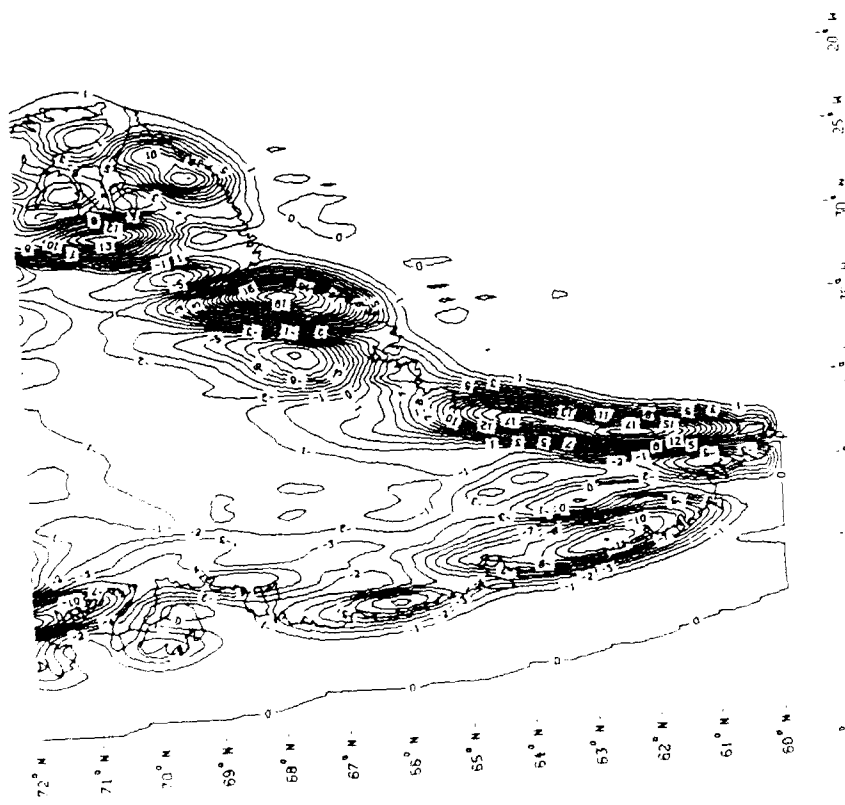


FIGURE 17. VERTICAL DEFLECTION η AT 3800 M BY TOPOGRAPHIC REDUCTION. CONTOUR INTERVAL IS 1 ARCSEC.

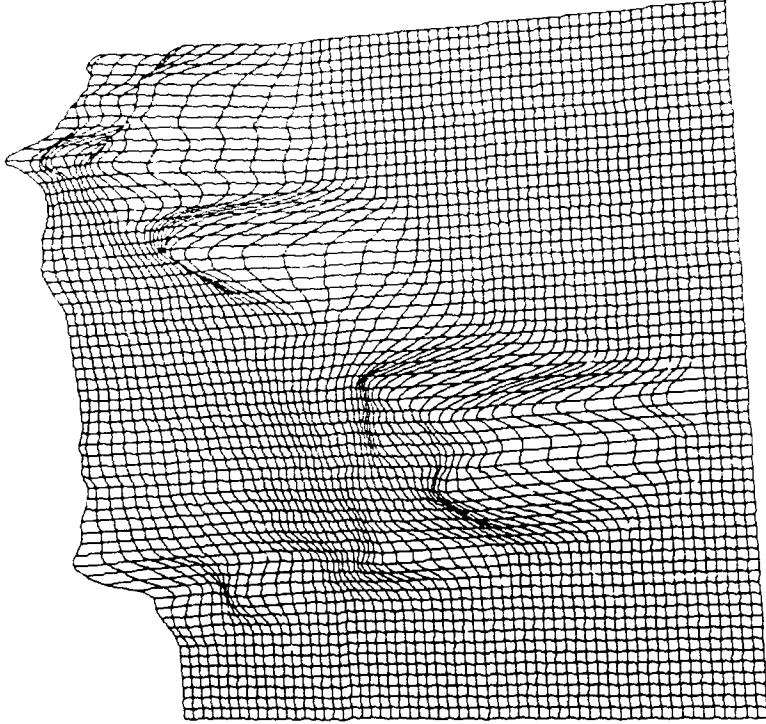


FIGURE 18. 3D PERSPECTIVE OF GRAVITY DISTURBANCE AT 3800 M. VIEW IS FROM SSW.

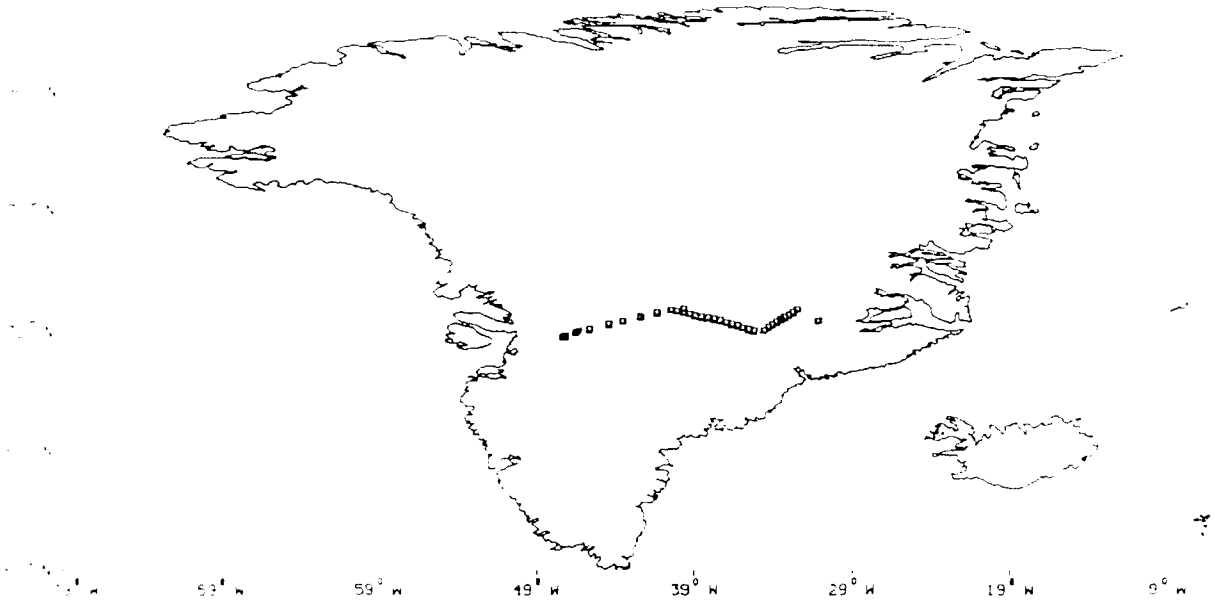


FIGURE 19. NRL GRAVITY ANOMALY PROFILE
NEAR 70.4° N

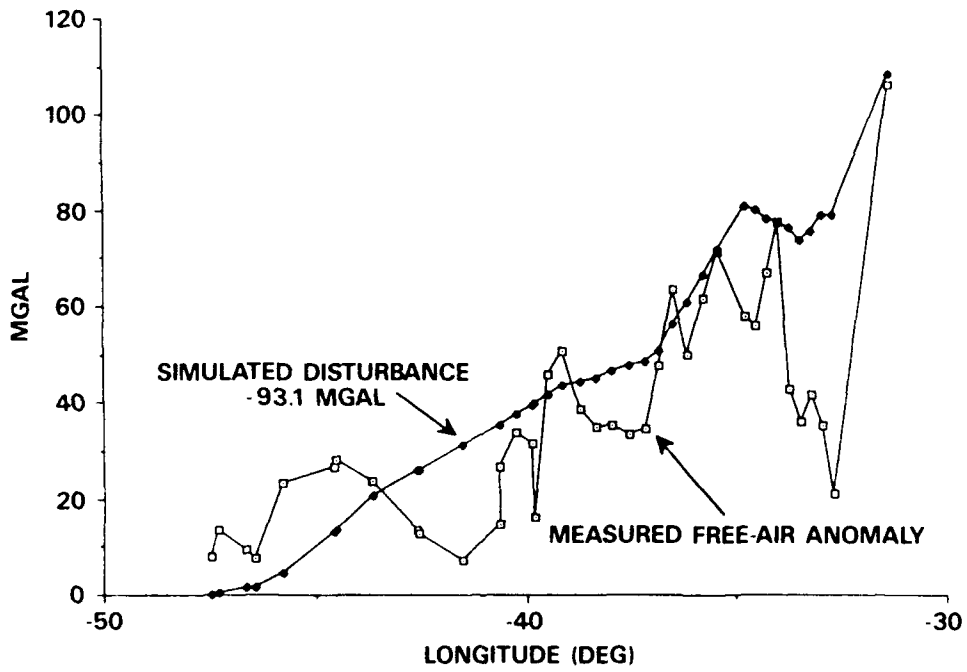


FIGURE 20. ACTUAL ANOMALY VS SIMULATED
DISTURBANCE ALONG NRL PROFILE



FIGURE 21. DMAAC GRAVITY ANOMALY PROFILE NEAR 66.4°N

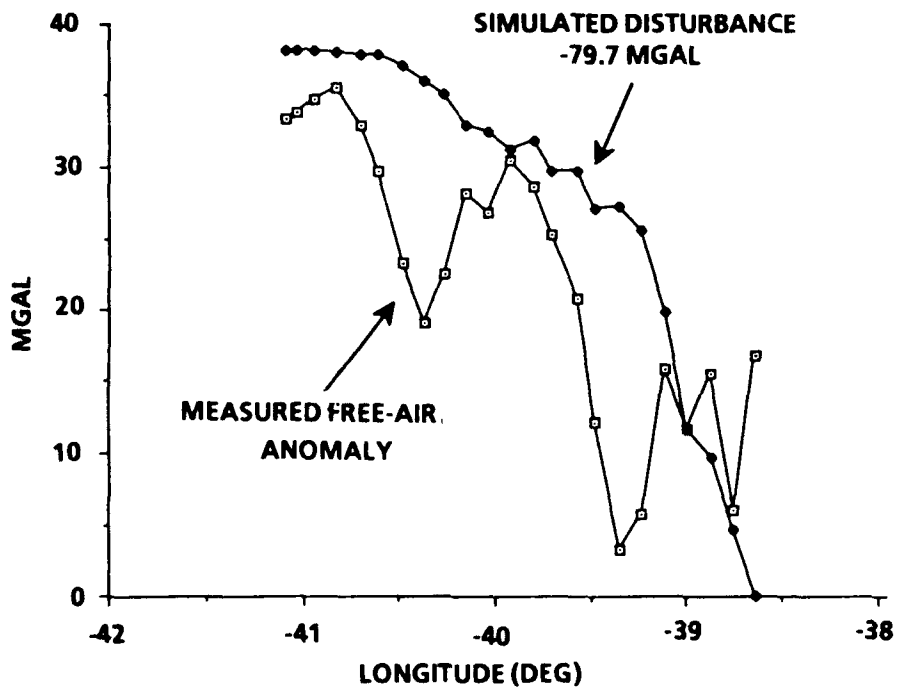


FIGURE 22. ACTUAL ANOMALY VS SIMULATED DISTURBANCE ALONG DMAAC PROFILE

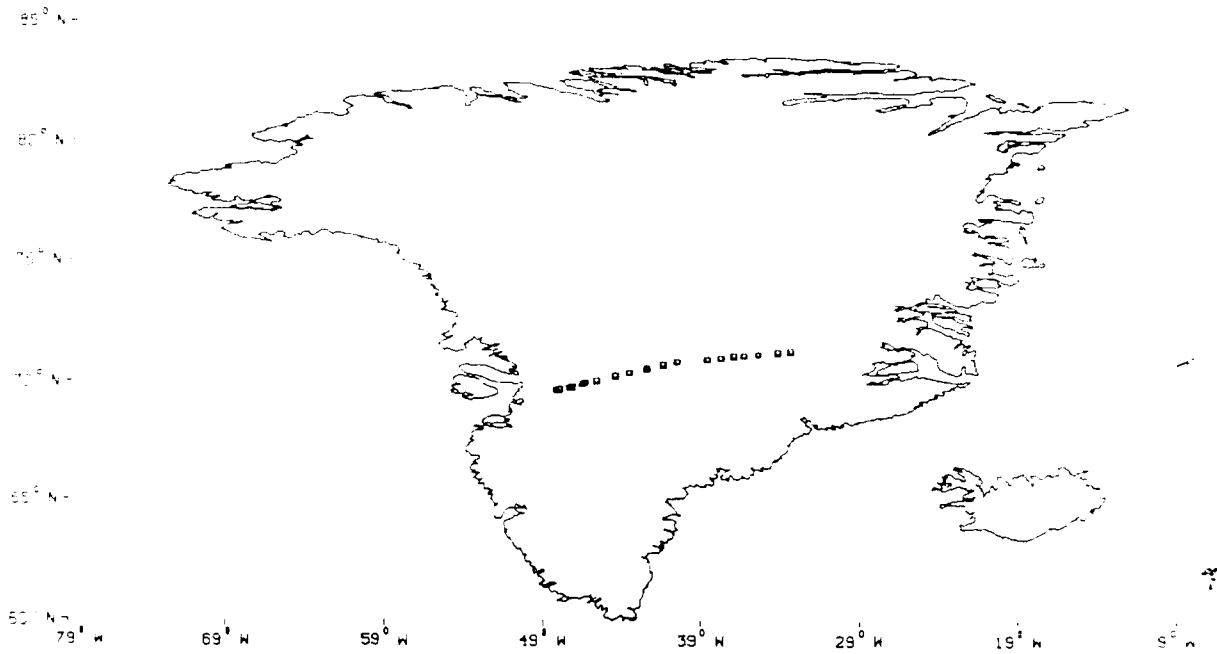


FIGURE 23. NRL GRAVITY ANOMALY PROFILE NEAR 70.5° N

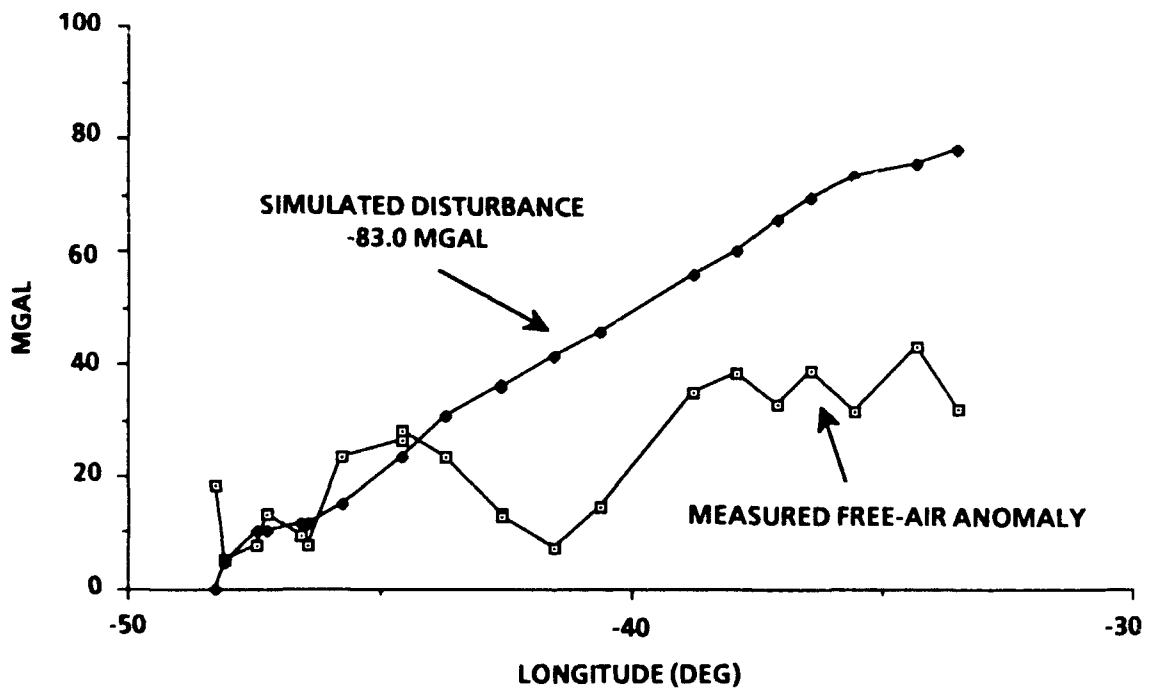


FIGURE 24. ACTUAL ANOMALY VS SIMULATED DISTURBANCE ALONG NRL PROFILE

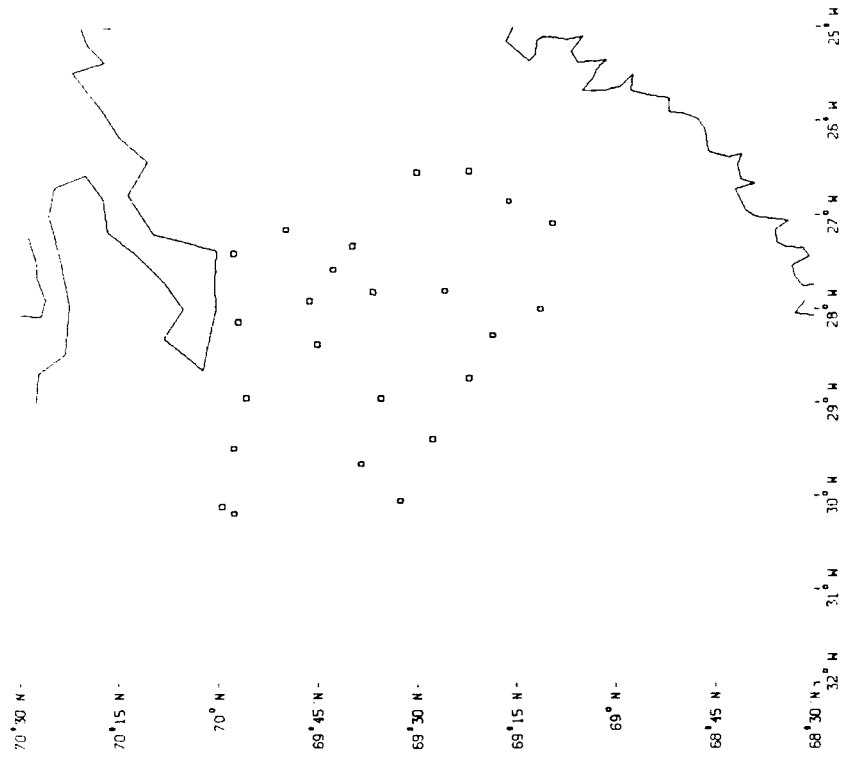


FIGURE 25. GÅSEFJORD LOCATION OF
NRL FREE-AIR ANOMALIES

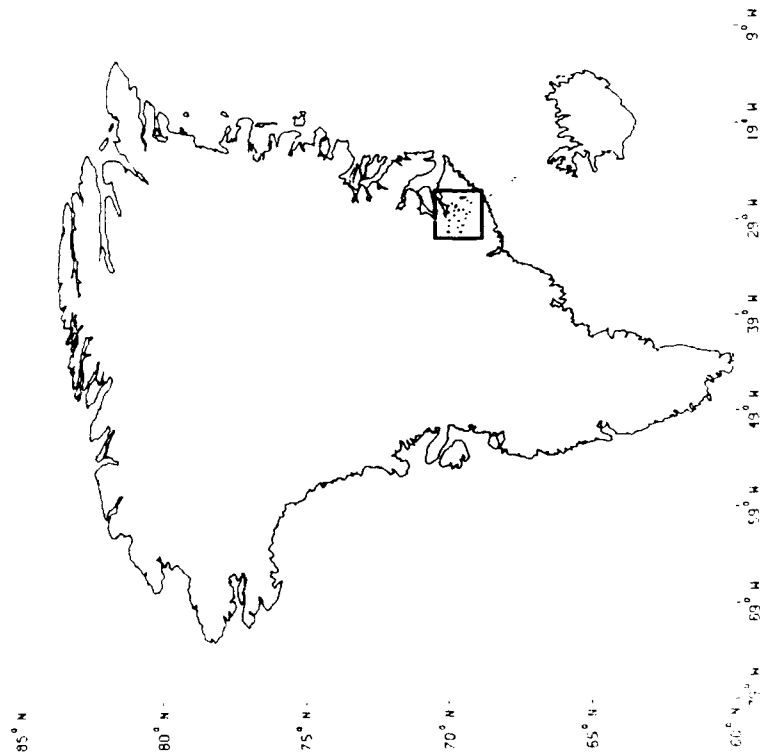


FIGURE 26. GÅSEFJORD DISTRIBUTION OF
NRL FREE-AIR ANOMALIES

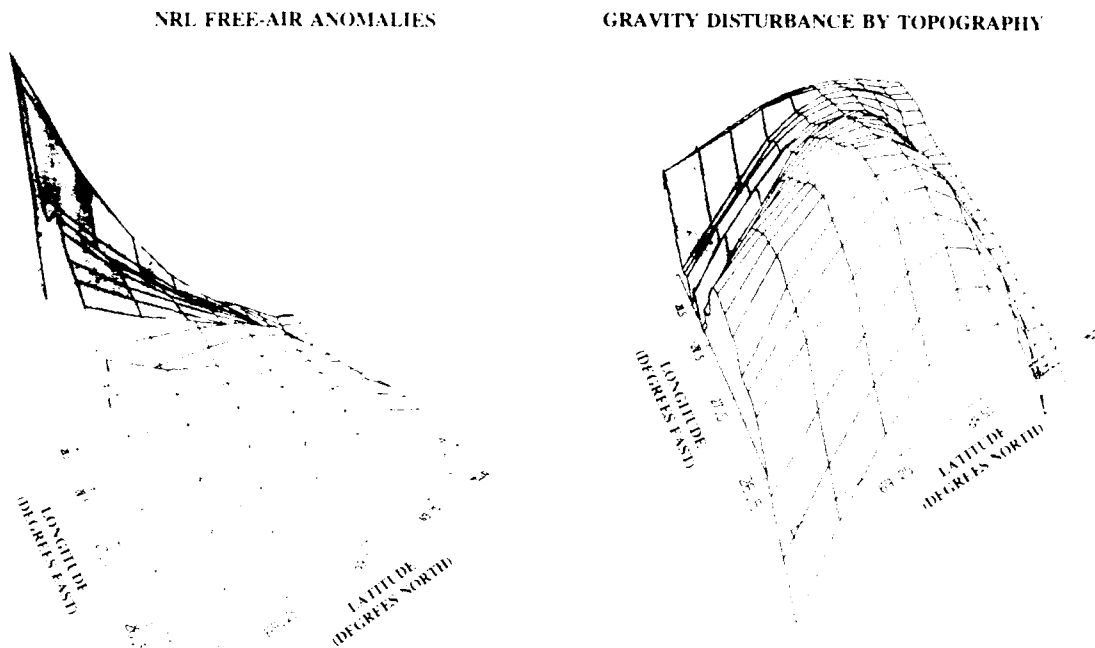


FIGURE 27. GÅSEFJORD 3D PERSPECTIVE OF FREE-AIR AND SIMULATED GRAVITY. VIEW IS FROM SSE. SHADED AREAS LACK DATA AND ARE PROBABLY INACCURATE. VERTICAL SCALE 1 = 15 MGAL.

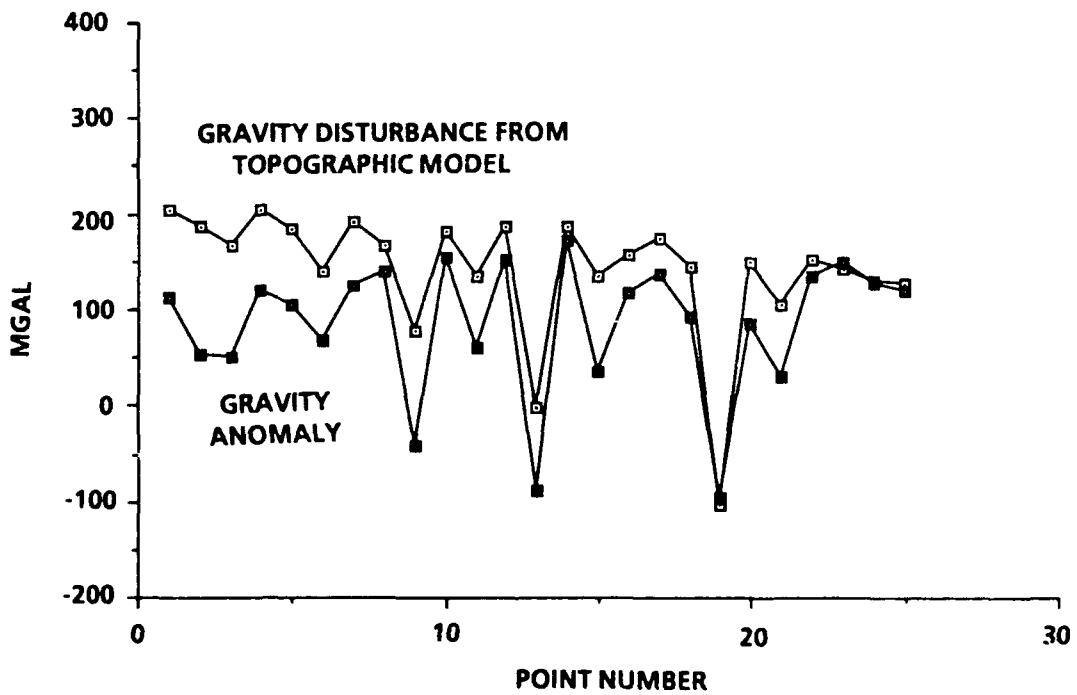


FIGURE 28. MODEL COMPARISON IN GÅSEFJORD AREA

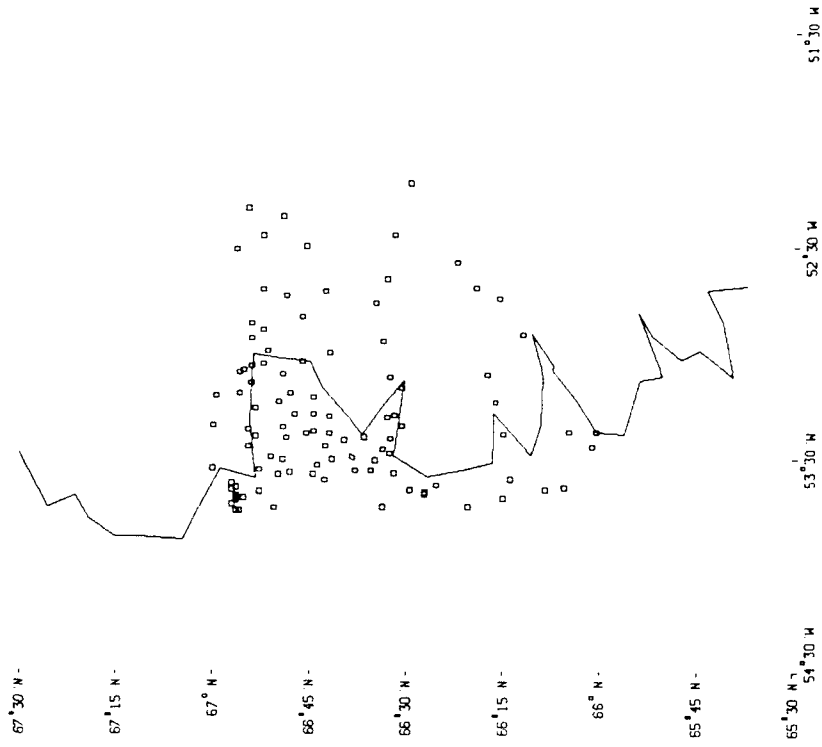


FIGURE 30. HOLSTEINSBORG DISTRIBUTION OF
NRL FREE-AIR ANOMALIES



FIGURE 29. HOLSTEINSBORG LOCATION OF
NRL FREE-AIR ANOMALIES

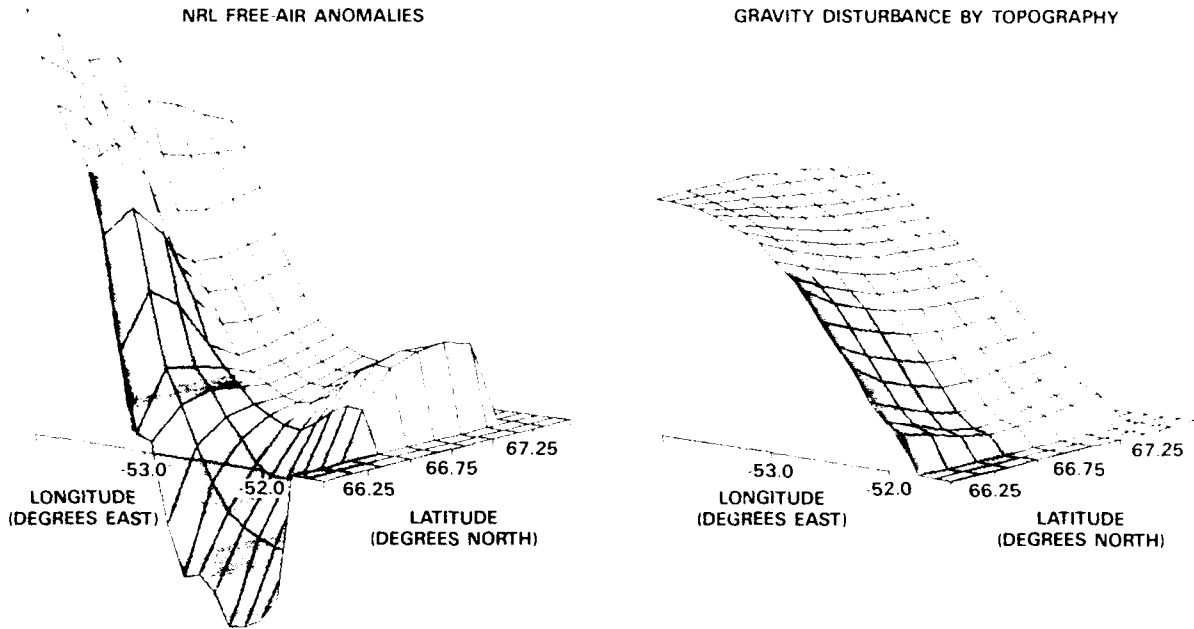


FIGURE 31. HOLSTEINSBORG 3D PERSPECTIVE OF FREE-AIR AND SIMULATED GRAVITY. VIEW IS FROM ESE. SHADED AREAS LACK DATA AND ARE PROBABLY INACCURATE. VERTICAL SCALE $I = 7$ MGAL.

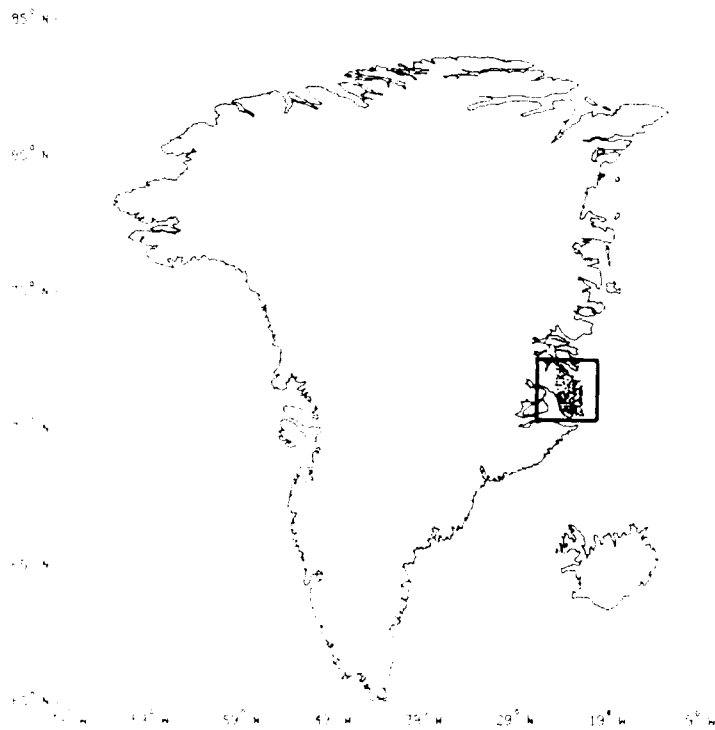


FIGURE 32. JAMESON LAND LOCATION OF NRL FREE-AIR ANOMALIES



FIGURE 33. JAMESON LAND DISTRIBUTION OF
NRL FREE-AIR ANOMALIES

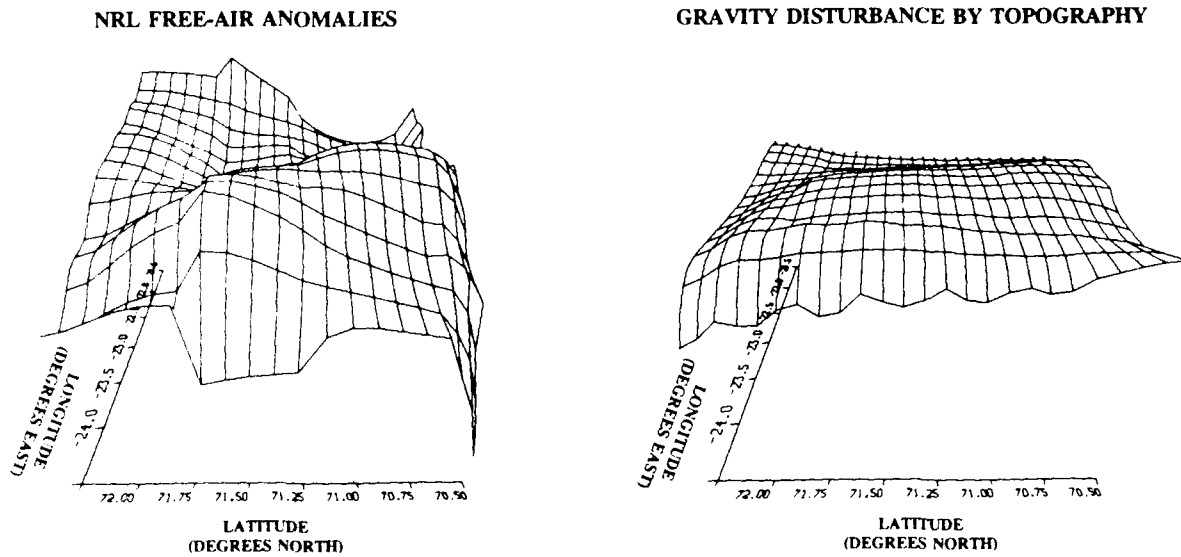


FIGURE 34. JAMESON LAND 3D PERSPECTIVE OF FREE-AIR
AND SIMULATED GRAVITY. VIEW IS FROM WEST.
VERTICAL SCALE 1 = 15 MGAL.

DISTRIBUTION

	<u>Copies</u>		<u>Copies</u>
ATTN K BURKE (PPG)	1	ATTN G MADER	1
W WOODEN (PRA)	1	NGS/NOS/NOAA N/CG114	
DIRECTOR		6001 EXECUTIVE BLVD	
DEFENSE MAPPING AGENCY		ROCKVILLE MD 20852	
HEADQUARTERS			
BLDG 56			
US NAVAL OBSERVATORY		ATTN R RAPP	1
WASHINGTON DC 20305-3060		DEPT OF GEODETIC SCIENCE	
		AND SURVEYING	
		THE OHIO STATE UNIVERSITY	
ATTN L DOTSON (DSG)	5	1958 NEIL AVE	
DIRECTOR		COLUMBUS OH 43210	
DEFENSE MAPPING AGENCY			
AEROSPACE CENTER			
3200 S SECOND ST			
ST LOUIS MO 63118-3399			
		ATTN CODE 671	
		R BINDSCHADLER	1
ATTN R ZIEGLER (SGS)	5	H ZWALLY	1
M KUMAR (SGS)	1	CODE 626	
DIRECTOR		J MARSH	1
DEFENSE MAPPING AGENCY		CODE 920	
SYSTEMS CENTER		H FREY	1
STE 800		NATIONAL AERONAUTICS AND	
8301 GREENSBORO DR		SPACE ADMINISTRATION	
MCLEAN VA 22102		GODDARD SPACE FLIGHT CENTER	
		GREENBELT MD 20771	
ATTN J BROZENA	5		
M PETERS	1		
P VOGT	1	ATTN A BRENNER	1
NAVAL RESEARCH LABORATORY		ST SYSTEMS INC	
MAIL CODE 5110		9701 L PHILADELPHIA COURT	
4555 OVERLOOK AVE SW		LANHAM MD 20706	
WASHINGTON DC 20375			
ATTN S BARKER	5	ATTN J MAJOR	1
M CHALONA	1	ST SYSTEMS INC	
COMMANDING OFFICER		4400 FORBES BLVD	
NAVAL OCEANOGRAPHIC OFFICE		LANHAM MD 20706-9008	
CODE GG			
STENNIS SPACE CENTER MS 39522-5001			

DISTRIBUTION (CONTINUED)

	<u>Copies</u>
ATTN C HANSON WORLD DATA CENTER A FOR GLACIOLOGY NATIONAL SNOW AND ICE DATA CENTER CIRES CAMPUS BOX 449 UNIVERSITY OF COLORADO BOULDER CO 80309	1
ATTN A OHMURA GEOGRAPHISCHES INSTITUT ETH WINTERTHURERSTRASSE 190 CH 8057 ZURICH SWITZERLAND	1
DEFENSE TECHNICAL INFORMATION CENTER CAMERON STATION ALEXANDRIA VA 22304-6145	12
ATTN GIFT AND EXCHANGE DIV LIBRARY OF CONGRESS WASHINGTON DC 20540	4
INTERNAL DISTRIBUTION:	
E211 (GREEN)	1
E31 (GIDEP)	1
E231	3
E232	2
K10	1
K104 (DIDONATO)	1
K104 (FELL)	15
K105	2
K106	1
K107	4
K12	2
K12 (CUNNINGHAM)	15
K12 (GROEGER)	1
K12 (SEAY)	1
K13	2
K14	2
K40	1
K41 (RUFTY)	1
K43	2
K43 (BROWN)	1
K43 (SITZMAN)	5

REPORT DOCUMENTATION PAGE

Form Approved
OMB No 0704-0188

Public reporting burden for this collection of information is estimated to average 1 hour per response, including the time for reviewing instructions, searching existing data sources, gathering and maintaining the data needed, and completing and reviewing the collection of information. Send comments regarding this burden estimate or any other aspect of this collection of information, including suggestions for reducing this burden, to Washington Headquarters Services, Directorate for Information Operations and Reports, 1215 Jefferson Davis Highway, Suite 1204, Arlington, VA 22202-4302, and to the Office of Management and Budget, Paperwork Reduction Project (0704-0188), Washington, DC 20503.

1. AGENCY USE ONLY (Leave blank)	2. REPORT DATE July 1991	3. REPORT TYPE AND DATES COVERED Final	
4. TITLE AND SUBTITLE Forecasting Geopotential Trends in Southern Greenland		5. FUNDING NUMBERS	
6. AUTHOR(S) James P. Cunningham Patrick J. Fell		8. PERFORMING ORGANIZATION REPORT NUMBER NAVSWC TR 91-409	
7. PERFORMING ORGANIZATION NAME(S) AND ADDRESS(ES) Naval Surface Warfare Center (K12) Dahlgren, VA 22448-5000		10. SPONSORING/MONITORING AGENCY REPORT NUMBER	
9. SPONSORING/MONITORING AGENCY NAME(S) AND		10. SPONSORING/MONITORING AGENCY REPORT NUMBER	
11. SUPPLEMENTARY NOTES			
12a. DISTRIBUTION/AVAILABILITY Approved for public release; distribution is unlimited.		12b. DISTRIBUTION CODE	
13. ABSTRACT (Maximum 200 words) <p>Various data types including SEASAT and GEOSAT satellite radar altimetry and aircraft-collected radio echo soundings were used to develop a topographic data base for Greenland south of 72° N. The data base consists of the ice surface and underlying bedrock surface elevations in regular grids. These grids and given density structures provide models of the localized mass distribution above mean sea level and intermediate wavelengths of the geopotential. Contours of gravity disturbance and deflections of the vertical at altitude predicted using the model demonstrate provinces distinguished by their gravimetric gradients. Comparisons between modeled gravity disturbance and observed free-air anomalies show that intermediate wavelength trends in the anomalies are often predicted by the model. It is proposed that the geopotential model could aid in the design of an airborne geophysical survey of southern Greenland and in the interpretation of the survey data.</p>			
14. SUBJECT TERMS SEASAT GEOSAT satellite geophysical data Greenland gravity topography		15. NUMBER OF PAGES 45	
		16. PRICE CODE	
17. SECURITY CLASSIFICATION OF REPORT UNCLASSIFIED	18. SECURITY CLASSIFICATION OF THIS PAGE UNCLASSIFIED	19. SECURITY CLASSIFICATION OF ABSTRACT UNCLASSIFIED	20. LIMITATION OF ABSTRACT UL

GENERAL INSTRUCTIONS FOR COMPLETING SF 298

The Report Documentation Page (RDP) is used in announcing and cataloging reports. It is important that this information be consistent with the rest of the report, particularly the cover and its title page. Instructions for filling in each block of the form follow. It is important to *stay within the lines* to meet optical scanning requirements.

Block 1. Agency Use Only (*Leave blank*).

Block 2. Report Date. Full publication date including day, month, and year, if available (e.g. 1 Jan 88). Must cite at least the year.

Block 3. Type of Report and Dates Covered. State whether report is interim, final, etc. If applicable, enter inclusive report dates (e.g. 10 Jun 87 - 30 Jun 88).

Block 4. Title and Subtitle. A title is taken from the part of the report that provides the most meaningful and complete information. When a report is prepared in more than one volume, repeat the primary title, add volume number, and include subtitle for the specific volume. On classified documents enter the title classification in parentheses.

Block 5. Funding Numbers. To include contract and grant numbers; may include program element number(s), project number(s), task number(s), and work unit number(s). Use the following labels:

- | | |
|----------------------|------------------------------|
| C - Contract | PR - Project |
| G - Grant | TA - Task |
| PE - Program Element | WU - Work Unit Accession No. |

Block 6. Author(s). Name(s) of person(s) responsible for writing the report, performing the research, or credited with the content of the report. If editor or compiler, this should follow the name(s).

Block 7. Performing Organization Name(s) and address(es). Self-explanatory.

Block 8. Performing Organization Report Number. Enter the unique alphanumeric report number(s) assigned by the organization performing the report.

Block 9. Sponsoring/Monitoring Agency Name(s) and Address(es). Self-explanatory.

Block 10. Sponsoring/Monitoring Agency Report Number. (*If Known*)

Block 11. Supplementary Notes. Enter information not included elsewhere such as: Prepared in cooperation with...; Trans. of...; To be published in... When a report is revised, include a statement whether the new report supersedes or supplements the older report.

Block 12a. Distribution/Availability Statement. Denotes public availability or limitations. Cite any availability to the public. Enter additional limitations or special markings in all capitals (e.g. NOFORN, REL, ITAR).

- DOD - See DoDD 5230.24, "Distribution Statements on Technical Documents."
- DOE - See authorities.
- NASA - See Handbook NHB 2200.2
- NTIS - Leave blank

Block 12b. Distribution Code.

- DOD - Leave blank.
- DOE - Enter DOE distribution categories from the Standard Distribution for Unclassified Scientific and Technical Reports.
- NASA - Leave blank.
- NTIS - Leave blank.

Block 13. Abstract. Include a brief (*Maximum 200 words*) factual summary of the most significant information contained in the report.

Block 14. Subject Terms. Keywords or phrases identifying major subjects in the report.

Block 15. Number of Pages. Enter the total number of pages.

Block 16. Price Code. Enter appropriate price code (*NTIS only*)

Block 17.-19. Security Classifications. Self-explanatory. Enter U.S. Security Classification in accordance with U.S. Security Regulations (i.e., UNCLASSIFIED). If form contains classified information, stamp classification on the top and bottom of this page.

Block 20. Limitation of Abstract. This block must be completed to assign a limitation to the abstract. Enter either UL (unlimited or SAR (same as report)). An entry in this block is necessary if the abstract is to be limited. If blank, the abstract is assumed to be unlimited.